SISSA - SCUOLA INTERNAZIONALE SUPERIORE DI STUDI AVANZATI
TRIESTE
Strada Costiera 11

ISAS - INTERNATIONAL SCHOOL FOR ADVANCED STUDIES

MOLECULAR DYNAMICS SIMULATION OF GOLD USING THE GLUE MODEL

Thesis submitted for the degree of
"Magister Philosophiae"

CANDIDATE
Furio Ercolessi

SUPERVISOR
Prof. Erio Tosatti

October 1986

TRIESTE

International School for Advanced Studies
Trieste

MOLECULAR DYNAMICS SIMULATION OF GOLD USING THE GLUE MODEL

Thesis submitted for the degree of
"Magister Philosophiae"

CANDIDATE
Furio Ercolessi

SUPERVISOR
Prof. Erio Tosatti

October 1986

INDEX

CHAPTER I
GENERALITIES ON NON-TWO-BODY EFFECTS IN THE PROPERTIES OF GOLD

1.1. Introduction

Calculating ab initio the properties of a material is a very difficult task. Even if we are not interested in the electronic properties of the system, but only in ionic properties (for instance, vibrations or surface structures), we must fully take into account the electronic aspect of the problem. This is particularly true in the case of metals, where the conduction and valence electrons play a key role in determining the main characteristics of the bonding.

Simply stated, the problem we wish to solve is the following: given a set of N nuclei with some positions $\vec{r}_1 ,..,\vec{r}_N$ and linear momenta $\vec{p}_1 ,..,\vec{p}_N$, which are the forces that they experience ? Knowing the answer to this question would allow us to find the most stable structures in presence of surfaces or defects, simply by relaxing the nuclei until the forces reduce to zero. Moreover, it would be possible to perform computer simulation of systems at finite temperatures, thus exploring the statistical mechanical properties.

In the Born-Oppenheimer adiabatic approximation [1], the forces can be obtained by considering the nuclei as fixed and searching for the minimum energy state of the electronic system. The force acting on a nucleus is then determined as the gradient of the total energy respect to a displacement of that nucleus. After all nuclei have been moved accordingly to the forces computed in this way, the whole process may be iterated for the new configuration, thus performing a dynamical calculation. This approach, however, is computationally very expensive and not feasible when the number of particles is large.

A more efficient calculational scheme, where the adiabatic approximation is not required, is the recently appeared Car-Parrinello method [2]. In this scheme the time evolution of a system containing nuclei and electrons can be followed by using an unified Lagrangian equation of motion where the electrons are treated within the frame of density functional theory. However, even using modern supercomputers, it is not possible to follow this approach in problems involving a large number of particles (of the order of several hundreds or thousands), due to the great amount of computations required for each configuration. This is especially true for transition or noble metals like gold, where the simultaneous presence of core, valence and conduction electrons calls for a very finely grained mesh to represent adequately the rapid variations of the electron density in the material.

Therefore, there is still a need for simple and empirical calculational schemes, where the total potential energy of the system is a function only of the nuclei coordinates :

$$V = V(\vec{r}_1, \vec{r}_2, .., \vec{r}_N) \qquad (1)$$

Here, the electrons do not appear explicitly, but of course their presence is reflected in the form of V. The most common choice is to express V as a sum of pairwise interactions:

$$V = \frac{1}{2} \sum_{\substack{ij \\ (j \neq i)}} \phi(r_{ij}) \qquad (2)$$

where r_{ij} is the distance between nuclei i and j, and the factor 1/2 avoids double counting. The problem is now reduced to the determination of a single function of one variable, i.e. the pair potential $\phi(r)$. This is of course an enormous simplification in the description of a material, which allows us to perform computer simulations very easily.

However, we should consider now in which cases this approximation can be justified.

In rare gas solids, cohesion is due to the van der Waals attractive forces which do not exactly have a two-body nature, but can be treated as such to a good approximation. It is in fact well known that this kind of materials can in practice be described quite accurately using pair potentials, such as the Lennard-Jones potential [3].

On the other hand, the properties of a metal are dominated by the conduction electrons. How these electrons respond to ionic motions determines the form of the atomic interactions. Our problem is whether it is possible to describe these interactions in terms of two-body forces between ions or not.

Metals are divided in two general classes: simple and non-simple. Simple metals, like sodium, can be thought of as non-overlapping ions immersed in a sea of nearly-free conduction electrons. Each ion consists of a nucleus surrounded by closed shells of tightly bound core electrons. In pseudopotential theory the ions, treated as point charges, are screened by the conduction electrons which tend to follow the ions adiabatically. The result is that for several purposes the metal can be described by effective pairwise forces between the ions [4].

Non-simple metals, like transition metals, are more complex. The free atoms contain partially filled shells of d-electrons, and s and p valence electrons. When the atoms are brought together to form the metal, a rather complex band structure appears, with d-bands and sp-bands above and below the Fermi level. If we displace an ion, the rearrangement of the electrons cannot be described as a cloud of charge following the ion. Therefore, it is clear that the pairwise approximation will generally not work in the case of transition metals [4], although it may still serve for

some particular study, e.g., bulk phonons [5]. In any case, extracting an effective pair potential from first principles is difficult [4], and the usual choice consists in building it empirically by fitting known bulk properties of the material, such as the lattice constant, the cohesive energy, the phonon frequencies and so on. However, it will be shown in the next Section that there are some serious intrinsic drawbacks in the pair potential approach which prevent an accurate description of a non-simple metal like gold.

1.2. Failures of pair potentials in metallic materials

Let us define the dimensionless ratio $C = E_c / k_B T_m$, where E_c is the cohesive energy, T_m the melting temperature and k_B the Boltzmann constant. We can see from Table 1 that C is about 10 in rare gas solids, but around 30 in metals.

Using two-body forces, the cohesive energy is simply due to the bonds that must be broken to remove an atom, and can be easily calculated for a given crystal structure. For example, for a first-neighbours potential we have

Material	E_c	T_m	C	S_m	$\Delta V/V_s$
Neon	0.02	24	9.7	1.64	15.3
Argon	0.080	84	11.1	1.69	14.4
Krypton	0.116	117	11.5	1.69	15.1
Xenon	0.17	161	12.3	1.71	15.1
Aluminum	3.34	933	41.5	1.39	6.5
Lead	2.04	601	39.4	0.96	3.6
Nickel	4.435	1728	29.8	1.22	5.4
Palladium	3.936	1825	25.0	1.13	5.9
Platinum	5.852	2042	33.3	1.16	6.6
Copper	3.50	1357	29.9	1.16	4.2
Silver	2.96	1234	27.8	1.10	3.8
Gold	3.78	1336	32.8	1.13	5.2

Table 1

Cohesive energies (in eV/atom), melting temperatures (in degrees Kelvin), ratios $C=E_c/k_B T_m$, entropy changes on melting S_m (in k_B/atom) and volume changes on melting $\Delta V/V_s$ (in %) for several fcc solids. Cohesive energies are from ref. [6], all other data from ref. [7].

$$E_c = -\frac{\eta}{2}\phi(d)$$

where d is the first neighbour distance and η the coordination number (12 for the fcc structure). The melting temperature can be extracted from computer simulations (with the molecular dynamics technique). It turns out that the calculated C is always of the order of 10. This implies that in metals E_c and T_m cannot be reproduced simultaneously using pair potentials. A system with the correct cohesion is stiff compared to the real material and melts at a much higher temperature, while a system with a nearly correct T_m has a cohesion too low [5].

Table 1 shows also that metals have a low entropy change and volume change on melting when compared with rare gas solids. Again, these characteristics are not well reproduced by pairwise forces. For example, a system described by the Lennard-Jones potential $\phi=4\epsilon[(\sigma/r)^{12}-(\sigma/r)^{6}]$ has, at the triple point, C=12.8, $S_m=2.16\ k_B/atom$, $\Delta V/V_s=17.7\%$ [8].

Another difficulty with two-body potentials is that the vacancy formation energy E_v is nearly equal to the cohesive energy E_c. In fact, the energy required to create a vacancy is given by

$$E_v = E_N^* - E_N$$

where E_N is the total energy of a system with N particles in N crystal sites (no vacancy), and E_N^* is the total energy of a system with N particles in N+1 crystal sites, i.e. with a vacancy. In the pairwise scheme, if we neglect atom relaxations around the vacancy, we have

$$E_N^* - E_{N+1} = -\eta\,\phi(d)$$

$$E_{N+1} - E_N = -E_c = \frac{\eta}{2}\phi(d)$$

and therefore

$$E_v = -\frac{n}{2}\phi(d) = E_c$$

On the other hand, Table 2 shows that in metals E_v/E_c is about one third. The fact that it is relatively easy to create defects in the material is of course connected with the low melting temperature [13].

Another discrepancy between two-body and metallic systems is related to the so-called "Cauchy relation" between two of the three independent elastic constants in a cubic crystal :

$$C_{12} = C_{44} \qquad (3)$$

Its validity is a mathematical consequence of using pairwise central forces [14,15], but, as Table 3 shows, it is far from being satisfied in metals. The low value of C_{44}, which is one of the shear moduli, is related to the high ductility and malleability of these materials (in particular of gold).

Surface properties are also a quite severe test for the validity of interatomic forces. For example, it can be shown [17,18] that a two-body potential without oscillations, such as the classical Lennard-Jones or Morse poten-

Material	E_v	E_v/E_c	Ref.
Neon	0.021	1.05	[9]
Argon	0.076	0.95	[9]
Krypton	0.077	0.66	[9]
Aluminum	0.76	0.23	[10]
Lead	0.49	0.24	[11]
Nickel	1.39	0.31	[12]
Platinum	1.51	0.26	[10]
Copper	1.14	0.33	[10]
Silver	1.08	0.36	[10]
Gold	0.95	0.25	[10]

Table 2

Vacancy formation energies (in eV) and their ratios to the cohesive energies for several fcc solids.

Material	C_{11}	C_{12}	C_{44}	Ref.
Neon	0.0166	0.0086	0.0095	[16]
Argon	0.042	0.024	0.022	[16]
Krypton	0.051	0.028	0.027	[16]
Xenon	0.053	0.028	0.030	[16]
Aluminum	1.143	0.619	0.316	[6]
Lead	0.555	0.454	0.194	[6]
Nickel	2.612	1.508	1.317	[6]
Palladium	2.341	1.761	0.712	[6]
Copper	1.762	1.249	0.818	[6]
Silver	1.315	0.973	0.511	[6]
Gold	2.016	1.697	0.454	[6]

Table 3

Elastic constants at T=0°K (in 10^{12} dyne/cm^2) for several fcc solids.

tials, always leads to an outwards relaxation of the first surface layer (i.e., the distance between the first and the second layer exceeds the bulk interplanar distance). On the other hand, metals usually exhibit an inwards relaxation of the first layer [19] [*]. Moreover, it is clear that the occurrence of surface reconstructions cannot be explained by two-body schemes (unless, of course, a different potential is used for surface atoms [21]).

Another, perhaps more serious problem which occurs at surfaces of two-body systems is an extremely high evaporation rate near the melting temperature, as seen from molecular dynamics simulations [22,23]. This results in a very high value for the vapour tension. Again, this is a situation typical, for example, of rare gas solids but not of metal surfaces, where the evaporation rate is so low that no atoms leaving the surface should be seen at reasonable temperatures on the size and time scales used in computer simulations (of course, this is another aspect of the impossibility of obtaining at the same time a good cohesive energy and a good melting temperature). In summary, the surface

---

[*] Inwards relaxations can be predicted, however, by potentials with an oscillatory tail [18,20].

properties predicted by two-body potentials are generally vastly different from those of the real metal.

Some of the difficulties described above can be avoided by adding a volume-dependent term to the total potential energy [24,25]. In its simple form, this correction contains a term linear in the volume:

$$V = \frac{1}{2}\sum_{(j\neq i)}\sum_{ij}\phi(r_{ij}) + p_o\Omega \qquad (4)$$

where p_o is a constant and Ω the total volume of the system. In particular, it can be shown that by choosing

$$p_o = \frac{1}{2}(C_{12} - C_{44}) \qquad (5)$$

we obtain correct values for the elastic constants, i.e. the Cauchy relation no longer holds. For this reason, the quantity $(C_{12}-C_{44})/2$ is called the "Cauchy pressure". While this approach may be helpful for a better representation of the bulk, it raises new problems when applied on surfaces (external or internal, as in vacancies, cracks, ..), where the volume is not unambiguously defined [26,27].

Therefore, one is led to the conclusion that a scheme based on pair interactions does not describe a metal in an adequate way, in particular when surface properties are considered. In the next Chapter, an empirical many-body hamiltonian, which overcomes all the difficulties mentioned in this Section, will be introduced.

CHAPTER II
THE GLUE MODEL

2.1. The ``glue'' concept

As discussed in the previous Chapter, the presence of the conduction electrons in non-simple metals is responsible for the presence of non-two-body effects in the physical properties of these materials. Roughly speaking, these electrons constitute a sort of "glue" which accounts for the strong cohesive character of the metallic bond. An ion which is immersed in this "glue" can move around in a relatively easy way, but pulling an atom out of the system has a high energetic cost.

When attempting to model this situation, the key variable to consider is the local atomic coordination, i.e. the number of neighbours of a given ion. Assuming that the coordination around an ion represents in some way the amount of local electronic density, we can take this coordination as the variable characterizing the environment in which our ion is situated.

Then we can propose the following schematic picture of an ion moving inside the metal: when its coordination is nearly equal to the bulk coordination, the ion moves in a more or less "normal" way, interacting with the other ions through an effective two-body potential [28]. However, motions which tend to change the coordination in an appreciable way are greatly discouraged by their high energetic cost.

Such a mechanism cannot be modeled by two-body forces, for one simple reason: a two-body scheme implies a linear dependence of the energy of an atom upon its coordination. The strength of any alternative scheme should be based on the non-linearity of this dependence.

Let us consider, for example, the formation of a vacancy. In an fcc crystal structure, it implies the change in coordination of the 12 neighbouring atoms from 12 to 11. In our picture, this change is rather small and leaves almost unchanged the local environment, so the vacancy formation energy will be low. On the other hand, extracting a single atom from the system implies changing its coordination from 12 to 0. This is a dramatic change, and the associated energy cost (which is the cohesive energy) will be high. It is evident here that the difference between E_v and E_c is an expression of the non-linearity of the energy of an atom as a function of its coordination.

2.2. The glue hamiltonian

The concepts developed in the previous Section can be expressed in a mathematical form by writing as follows the total potential energy of a system of N particles (henceforth called "atoms"):

$$V = \frac{1}{2}\sum_{(j\neq i)ij} \phi(r_{ij}) + \sum_i U(n_i) \qquad (6)$$

A standard two-body part is still present, together with the new many-body term which replaces the volume-dependent term in eq. (4). Here, n_i is the coordination of atom i, which will be later defined in more detail. The function U(n) associates an energy value to this coordination, thereby including the previously discussed "gluing" effects of the conduction electrons. For this reason, U(n) has been nicknamed the "glue", and eq. (6) the "glue hamiltonian" [23,29,30].

It is natural to impose

$$U(0) = 0 \qquad (7)$$

In this way, the total energy is referred to that of a sys-

tem of N atoms at rest, infinitely far each from the other. Of course, we expect U(n) to be negative in the coordination range of our interest.

In order to use (6) in computer simulations, we need a procedure to compute n_i for each atom in the system. Since our purpose is to write a hamiltonian of the form (1), that is, where only the atom coordinates appear, it must be

$$n_i = n_i(\vec{r}_1, \vec{r}_2, \ldots, \vec{r}_N) \tag{8}$$

The simplest choice consists in building n_i as a superposition of contributions coming from the neighbours of atom i :

$$n_i = \sum_{(j \neq i)} \rho(r_{ij}) \tag{9}$$

where $\rho(r)$ is a short-ranged, monotonically decreasing function of the distance. Equation (9) essentially counts the number of neighbours of atom i. This is done in a continuous way, so that nearby atoms give a contribution to n_i larger than far atoms. The final result for n_i is a real number that generalizes the usual idea of coordination. This generalized coordination n_i is a dynamical variable of our hamiltonian.

It should be noted here that the units for ρ (and n) are arbitrary, because they are only auxiliary quantities in this scheme. In particular, given $\rho(r)$ and U(n), the new pair

$$\begin{aligned} \hat{\rho}(r) &= c\rho(r) \\ \hat{U}(n) &= U(n/c) \end{aligned} \tag{10}$$

describes the same physics, i.e., it gives rise to the same forces for an arbitrary value of c. So we have the freedom to define a scale for n. A convenient choice is to make it coincident with the ordinary coordination number for a bulk

atom. Assuming an fcc (or hcp) crystal structure, this means that we are at freedom to fix arbitrarily, but suggestively

$$n_e = 12 \tag{11}$$

where n_e indicates the result of applying eq. (9) to a bulk atom in an undistorted lattice. When $\rho(r)$ has a range limited to the first neighbours, it is $n_e = 12\rho(d)$ where d is the first neighbours distance, and therefore condition (11) becomes simply

$$\rho(d) = 1 \tag{12}$$

This normalization will be adopted from now on.

The glue hamiltonian is particularly convenient from the computational point of view, since the atomic positions appear only in the form of distances between pairs. In spite of the intrinsic many-body character of the glue, there are no explicit three-body or more complex terms in the expressions for the forces. In fact, the force $\vec{F}_i$ acting on a particle i is given by the following formula, obtained by derivation of eq. (6) (and using (9)):

$$\vec{F}_i = -\vec{\nabla}_i V = -\sum_j \phi'(r_{ij}) \frac{\vec{r}_{ij}}{r_{ij}} - \sum_j \left[U'(n_i)+U'(n_j)\right]\rho'(r_{ij})\frac{\vec{r}_{ij}}{r_{ij}} \tag{13}$$

where

$$\vec{r}_{ij} = \vec{r}_i - \vec{r}_j$$

and the prime indicates derivation. The extension of a standard molecular dynamics program to include the glue forces is relatively easy to accomplish, and is discussed in the Appendix.

Finally, let us note an interesting feature of eq. (13) [29,43,45]. If r_m is the cutoff range associated to $\rho(r)$,

it is clear that $\vec{F}_i$ depends on the value of n_j for all atoms j whose distance from i is less than r_m. But n_j, in turn, depends on the positions of all atoms k within a distance r_m from j. Thus, the position of an atom k at a distance up to $2r_m$ from an atom i has a direct influence on the force acting on i, so that the "effective interaction range" of the glue forces is twice the range of $\rho(r)$. In an fcc structure, this means that a first-neighbours ranged $\rho(r)$ can couple together neighbours up to the seventh shell.

2.3. Physical interpretations: embedded-atom-method and tight-binding models

We have introduced the glue hamiltonian from a purely empirical point of view. However, it should be pointed out that some alternative approaches lead to the same scheme for the hamiltonian by starting from first principles considerations. In particular, two families of such approaches can be found in literature: one is the "embedded-atom-method" (or EAM), the other is in connection with the tight-binding model.

Daw and Baskes [31,32] have introduced this hamiltonian within the frame of density-functional theory. It has been subsequently used to study a wide range of bulk and surface properties of solid and liquid metals and of alloys [31-38]. In their interpretation, each atom of the metal is seen as an "impurity" embedded in a host system consisting of all other atoms. In the density-functional theory framework, using the uniform density approximation [39,40], the energy of this impurity can be written as a function of the host electron density (i.e., before the introduction of the impurity) $n_h(\vec{r})$ at the impurity site $\vec{R}$:

$$E_{imp} = F(n_h(\vec{R}))$$

Starting from this observation, Daw and Baskes take the fol-

lowing ansatz for the total energy of the system:

$$E_{tot} = \sum_i F(n_i)$$

where n_i is the electron density at the site of atom i of a system in which atom i is missing.

Two further assumptions are required:

1) A two-body part is also needed to account for the core-core repulsion. The potential is assumed to be purely repulsive.
2) n_i can be approximatively constructed as a superposition of atomic densities:

$$n_i = \sum_{(j \neq i)} \rho(r_{ij})$$

Here, $\rho(r)$ is the electron density distribution of a free atom, taken from Hartree-Fock calculations [41,42].

The resulting hamiltonian is thus formally identical to the glue hamiltonian. However, due to the large number of approximations involved, this connection with first principles cannot be of too much practical help in finding the optimal functions for a given metal, so that it remains necessary to resort to an empirical fit procedure.

The main practical difference between this scheme (called by Daw and Baskes "embedded-atom-method") and our glue, is that the function $\rho(r)$ is fixed in the EAM, while it is available for the fit procedure in the glue scheme. We have used this additional freedom to characterize well the thermal behavior and the surface properties of the system, as discussed in Section 2.7. A more "philosophical" difference is that n is the electronic density in the EAM, while in the glue scheme it is simply an auxiliary variable which is not identified with a precise physical quantity.

A hamiltonian based on the same spirit as the glue hamiltonian has been proposed by Finnis and Sinclair [43] for use in bcc transition metals. This model has been used to calculate vacancy and surface energies [43-45]. The Finnis and Sinclair hamiltonian is a glue hamiltonian where the glue has the analytic form

$$U(n) = -A\sqrt{n}$$

while $\phi(r)$ and $\rho(r)$ are built empirically. This particular form for U(n) comes from the second moment approximation to the tight binding model [46,47]. A similar scheme has recently been used by Tománek and Bennemann to study surface reconstructions [48].

2.4. A ''gauge invariance'' in the glue hamiltonian

In some of the "first principles" derivations described above, the glue part supplies the electronic cohesion while the two-body potential simulates the core-core repulsion between the ions. While this physical distinction seems appealing, it will be shown in this Section that no such distinction really exists when considering the glue hamiltonian in practice, because of the existence of a peculiar, gauge-like, invariance property.

Let us consider the full expression for the total potential energy:

$$V = \frac{1}{2}\sum_{\substack{ij \\ (j\neq i)}} \phi(r_{ij}) + \sum_i U\left(\sum_{\substack{j \\ (j\neq i)}} \rho(r_{ij})\right) \qquad (14)$$

If U is a linear function of n:

$$U(n) = \lambda n \qquad (15)$$

then (14) reduces to a two-body expression:

$$V = \frac{1}{2}\sum_{(j\neq i)}^{ij} \psi(r_{ij}) \tag{16}$$

where the "effective potential" $\psi(r)$ is given by

$$\psi(r) = \phi(r) + 2\lambda\rho(r) \tag{17}$$

Therefore, a glue term which is a linear function of coordination is equivalent to a two-body term; the physical meaning of this statement has been already discussed in Section 2.1.

We can go a little further by enunciating the following "gauge invariance" property of the glue hamiltonian:

A glue hamiltonian defined by $\phi(r)$, $U(n)$, $\rho(r)$ gives rise to forces which remain unchanged when these functions are replaced by $\phi^*(r)$, $U^*(n)$, $\rho(r)$, where

$$\begin{aligned} \phi^*(r) &= \phi(r) + 2\lambda\rho(r) \\ U^*(n) &= U(n) - \lambda n \end{aligned} \tag{18}$$

and λ is an arbitrary real number.

The demonstration is straightforward: in going from ϕ,U,ρ to ϕ^*,U^*,ρ, we add and subtract the same quantity in the expression (14). This situation is reminiscent of the "gauge invariance" of electromagnetic potentials in classical electromagnetism.

This has some practical consequences. In particular, there is no unique choice for ϕ and U, since a term linear in the coordination can be transferred from the two-body part to the glue part and viceversa without any change in the physics. For instance, one may have a system where the two-body potential is purely repulsive and all the attraction is supplied by the glue; at the equilibrium lattice spacing, these two forces balance exactly. But with the appropriate "gauge transformation" it is also possible to

construct a completely equivalent hamiltonian where both the two-body part alone and the glue part alone predict the same, equilibrium lattice spacing.

Therefore, in spite of the physical reasoning which led us to conceive the glue U(n) and the glue hamiltonian, we are not able to attach a physical meaning to either U(n) or $\phi(r)$ when considered separately. More generally, we can state that, as usual, only gauge-invariant quantities can be connected to physical properties.

Some examples of gauge invariants are $\rho(r)$ itself, the second derivative of the glue U"(n), and the "effective potential" [29,32,43]

$$\psi(r,n) = \phi(r) + 2U'(n)\rho(r) \qquad (19)$$

Another obvious consequence of the "gauge invariance" is that a "gauge condition" can be arbitrarily imposed, thereby removing the ambiguity. A particularly convenient choice is

$$U'(n_0) = 0 \qquad (20)$$

With this condition, U(n) has a minimum in correspondence with the bulk coordination n_0, and for this reason it will be called the "bulk gauge". From a purely practical point of view, working in the bulk gauge has the advantage of making easier the fitting process. In particular, as it will be shown in the next Section, with this choice the transverse phonon frequencies depend only on the two-body potential. From now on, condition (20) will be assumed to hold.

2.5. Fitting the hamiltonian free functions to physical properties

In this Section, we derive some relations connecting the glue hamiltonian with a certain number of physical quantities. These relations will be useful in building ϕ, ρ, U by fitting these quantities to the experimental values for a given material. The following will be assumed:

- an fcc crystal structure
- a first-neighbours range for $\phi(r)$ and $\rho(r)$
- the normalizations (11) and (12) for n and ρ : $n_o=12$, $\rho(d)=1$
- the "bulk gauge" (20): $U'(n_o)=0$

These restrictions allow us to write simple formulas, which will be used in Sec. 2.8 to fit the hamiltonian to the experimental data for gold. More general formulas can be found in refs. [29] and [32].

Let us consider the potential energy per atom in a perfect lattice where R is the first-neighbours distance:

$$E(R) = \frac{12}{2}\phi(R) + U(12\rho(R))$$

In the general case the system is not in equilibrium, so that there is a net pressure

$$p(R) = -\frac{dE}{d\Omega_o} = -\frac{\sqrt{2}}{3R^2}\frac{dE}{dR} = -\frac{2\sqrt{2}}{R^2}\left[\phi'(R)+2\rho'(R)U'(12\rho(R))\right]$$

where $\Omega_o=R^3/\sqrt{2}$ is the volume occupied by an atom. Of course, when R is equal to the equilibrium distance d this pressure vanishes:

$$p(d) = -\frac{2\sqrt{2}}{d^2}\left[\phi'(d) + 2\rho'(d)U'(12)\right] = 0$$

Since we are adopting the bulk gauge, this condition reduces to the ordinary equilibrium condition for two-body potentials

$$\phi'(d) = 0 \qquad (21)$$

E(R) has a minimum for R=d, which is, apart of the sign, the cohesive energy:

$$E_c = - E(d) = -\left[6\phi(d) + U(12)\right] \qquad (22)$$

Finally, the bulk modulus of the system is given by

$$B = -\Omega_o \frac{dp}{d\Omega_o} = \Omega_o \frac{d^2E}{d\Omega_o^2} = \frac{\sqrt{2}}{9d} \left.\frac{d^2E}{dR^2}\right|_{R=d} =$$

$$= \frac{2\sqrt{2}}{3d} \phi''(d) + \frac{16\sqrt{2}}{d} \left[\rho'(d)\right]^2 U''(12) \qquad (23)$$

Equations (21), (22) and (23) give us three relations that can be used in the fit.

Eq. (23) deserves some extra comments. It can be shown [29], by calculating the dynamical matrix for the glue hamiltonian, that in the bulk gauge [*] the glue term does not have any effect on the transverse phonon frequencies: that are completely determined by the two-body potential. This fact can be intuitively understood by noting that the atomic density (or the coordination in our scheme) remains roughly constant in a transverse mode, while it is strongly modulated in a longitudinal mode. This fact implies that the elastic constants associated to the transverse modes in the limit $\vec{k} \rightarrow 0$, which are the shear moduli C_{44} and $(C_{11}-C_{12})/2$ or a combination of them, are also determined only by the two-body part. Therefore, the expressions obtained for a two-

---

[*] The following results can be expressed in a general gauge by substituting the two-body potential $\phi(r)$ with the effective potential (19) calculated for n=12.

body system [49,24]

$$C_{44} = \frac{\sqrt{2}}{2d}\,\phi''(d) \tag{24}$$

$$\frac{1}{2}(C_{11}-C_{12}) = \frac{\sqrt{2}}{4d}\,\phi''(d) \tag{25}$$

are still valid when the glue term is added. If we rewrite eq. (23) by expressing B in terms of the three elastic constants

$$B = \frac{1}{3}(C_{11}+2C_{12}) = \frac{2\sqrt{2}}{3d}\,\phi''(d) + \frac{16\sqrt{2}}{d}\left[\rho'(d)\right]^2 U''(12) \tag{26}$$

then we can solve for the elastic constants the linear system composed by (24), (25) and (26). It turns out that the many-body term in the expression for the bulk modulus is what has been called "the Cauchy pressure" in Section 1.2:

$$\frac{1}{2}(C_{12}-C_{44}) = \frac{8\sqrt{2}}{d}\left[\rho'(d)\right]^2 U''(12) \tag{27}$$

Therefore, the glue hamiltonian removes the Cauchy discrepancy in the elastic constants. It may be noted here that a system based <u>exclusively</u> on many-body forces of the glue type would have $C_{44}=0$, $C_{11}=C_{12}$, and therefore it would be unstable under shear deformations: two-body forces remain essential for a faithful description of the physical system. In other words, realistic two-body forces are such that they can not be "gauged away".

As stated above, the glue term does not have any effect on the transverse phonon frequencies. Moreover, it has been shown [29] that it does not have any effect for all $\vec{k}$ points that lie on the Brillouin zone boundaries. Therefore, all the phonon frequencies at the standard points of the Brillouin zone can be expressed in terms of the two-body potential. The relations are the following [49,24]:

Point X, branch L : $M\omega^2 = 8\phi''(d)$ (28)

Point X, branch T : $M\omega^2 = 4\phi''(d)$ (29)

Point W, branch π : $M\omega^2 = 6\phi''(d)$ (30)

Point W, branch Λ : $M\omega^2 = 4\phi''(d)$ (31)

Point L, branch L : $M\omega^2 = 8\phi''(d)$ (32)

Point L, branch T : $M\omega^2 = 2\phi''(d)$ (33)

where M is the atomic mass. All these frequencies, as well as the shear moduli, depend on a single parameter, namely $\phi''(d)$. Clearly, some kind of compromise must be adopted in the fitting process.

The glue hamiltonian solves the problem of the low vacancy formation energy compared to the cohesive energy; in fact the former, neglecting relaxations, is the energy associated with the breaking of 12 bonds, and the change of coordination of the 12 neighbour atoms from 12 to 11:

$$E_v = -6\phi(d) + 12\left[U(11)-U(12)\right] \qquad (34)$$

while the latter is given by (22). The two quantities differ by virtue of the non-linearity of the glue.

To conclude this Section, the surface energy per atom on a (111) unrelaxed fcc face is obtaied by removing 3 bonds and changing the coordination from 12 to 9:

$$E_s = -\frac{3}{2}\phi(d) + U(9) - U(12) \qquad (35)$$

Of course, these energies will be further lowered by relaxation effects, as will be discussed in detail later on.

2.6. A comment on the lack of angular forces

It follows from the results of the previous Section that from the point of view of fitting the lattice vibration spectrum a glue hamiltonian is not substantially better than

a two-body description. The origin of this difficulty lies in the fact that the glue is central, or non-directional, i.e. the glue energy depends only on the number of neighbours around an atom, while how these neighbours are disposed is not relevant. On the other hand, we expect that in real materials different angular arrangements of the atoms should make a significant difference to the energy. This picture is supported by the fact that it is possible to obtain an excellent agreement between the calculated and the experimental phonon dispersion relations by using three-body force constants with an angular dependence [50,51].

Another consequence of the lack of angular forces in the glue scheme is that, if the interaction range is limited to the first or second neighbours, the fcc and hcp crystal structures are predicted to have the same energy [26]. This is due to the fact that in these crystal structures the first two shells contain the same number of neighbours (respectively 12 and 6) at the same distances. On the other hand, there is a difference in the angular disposition of the second neighbours, and from a physical point of view this, rather than the different number of third neighbours, is likely to be the origin of the fcc-hcp energy difference.

This spherical symmetry is perhaps the most important shortcoming of the glue hamiltonian when compared to other empirical many-body schemes. However, the simplification, resulting in a saving of computing power for a molecular dynamics or MonteCarlo simulation, is enormous, and can hardly be underestimated.

2.7. The necessity of stringent tests: thermal and surface properties

There is obviously a large amount of arbitrariness in the glue hamiltonian, which so far is specified by three continuous functions, rather than by a handful of parameters. While the relations given in Section 2.5 provide some

fit points for $\phi(r)$, $\rho(r)$, U(n) or their derivatives at certain fixed values of the arguments, there remains a large freedom in the shape of these functions far from these fitting points. Therefore, it is possible to construct many different triplets of functions ϕ, ρ, U, all of which fit the same quantities (lattice spacing, cohesive energy, bulk modulus ...), yet describe different physical systems. It may be said that in this freedom lie both the strength and the weakness of the glue hamiltonian. One can confidently hope to find in the large space of all the possible choices a realization with overall properties similar to those of the real material. However, in order to restrict the number of candidates, some powerful selective tests need to be introduced. These tests, of course, should be able to extract new informations from the hamiltonian by probing more properties than those that have been fitted.

Thermal properties constitute the most useful test bench. In fact, when the atoms vibrate they sample wide regions of the three functions ϕ,ρ,U, so that the behavior of the system depends on their whole shape, even relatively far from the fit points. The "thermal test" is particularly severe at high temperatures, where anharmonic effects play an important role. Properties like the thermal expansion coefficient or the melting temperature are very sensitive to tiny details in the shape of ϕ,ρ and U. For instance, the slope of the core region in the two-body potential turns out to be crucial in determining the melting temperature. Moreover, a crystal structure which is found to be stable at T=0 with a certain glue hamiltonian, may, if allowed to, undergo a transition towards another structure at a finite temperature. If this is not the case for the real material, such a hamiltonian must be rejected.

Of course, investigating the thermal properties requires the use of a molecular dynamics or MonteCarlo simulation already during the construction phase of the glue

hamiltonian, just to try out successive realizations and discard the bad ones.

Another stringent test for a glue hamiltonian is the accurate description of defects, and in particular of surface properties. The interactions between surface atoms are very different from those between bulk atoms, because the coordination is lower and therefore a different part of U(n) becomes relevant. The resulting relaxation effects tend usually to reduce the bond lengths, so that also the behavior of $\phi(r)$ and $\rho(r)$ at distances lower than the bulk first neighbours distance is important in determining the final structure. For example, the amount of first-layer contraction, when experimentally known, may be another independent quantity that can be fitted. In materials which exhibit surface reconstructions, like gold, the reconstructed surface should have a surface energy lower than the non-reconstructed surface; and the contrary should occur in materials whose surfaces do not reconstruct.

Thermal and surface properties depend on the details of the glue hamiltonian in a complex way, so they are not easy to fit. However, by using molecular dynamics and a trial-and-error approach, it is possible to reproduce them rather accurately. This work requires a suitable parametrization of ϕ, ρ, U, flexible enough to allow shape variations of the functions within the constraints given by the fit points.

To conclude, it should be emphasized that we are generally unable (and unwilling) to determine an "optimal" realization of the glue. The search for a hamiltonian, conducted following the guidelines depicted above, terminates when a "satisfactory" realization is found; i.e., when some previously defined "design goals" have been attained within a reasonable margin. In particular, the three functions are not expected to be meaningful for values of their arguments outside of the range sampled in simulations (e.g., r deep in

the core region, n near 0 or extremely large, etc.). In fact, changing the functions in these regions does not modify the behavior of the system, when tested under normal conditions.

2.8. Construction of a glue hamiltonian for gold

In the fitting procedure described in this Section, the four conditions listed at the beginning of Sec. 2.5 have been adopted, so all the relations there reported can be applied. It should be noted that

1) an fcc structure is assumed as a starting point, but its stability is not guaranteed and therefore it must be verified.

2) the first-neighbours range for $\phi(r)$ and $\rho(r)$ a posteriori proved to be a valid choice in the case of gold; but this does not imply that such a short range is adequate for all the materials.

The following experimental data have been fitted exactly :

- T=0 lattice parameter, $a_0 = 4.0704$ Å.
- Cohesive energy, $E_c = 3.78$ eV/atom [6].
- Surface energy, $\sigma = 96.8$ meV/Å^2 [52]. This value has been fitted on a not reconstructed but relaxed (111) face. This case has been considered to be quite typical in the case of gold, where all surfaces reconstruct in order to achieve a closely-packed structure.
- Bulk modulus, $B = 1.803 \cdot 10^{12}$ dyne/cm^2 [53].
- Frequency of the transverse phonons at point X of the Brillouin zone, $\nu_T(X) = 2.75$ THz [54].

Moreover, we have attempted to reproduce at least reasonably (as explained in the previous Section) the following quanti-

ties:

- Vacancy formation energy, E_v = 0.95 eV [10].
- Thermal expansion coefficient, $\alpha = 15.8 \cdot 10^{-6} °K^{-1}$ at T=600°K [55].
- Melting temperature, T_m = 1336°K [55].
- Instability of the ideal surface structures (in particular, the (100) reconstruction which will be discussed in Chapter IV) [74].

As explained in Sec. 2.5, the phonon dispersion relations can be fitted only in an approximate way, because only two parameters are available. One of them is the bulk modulus; the other has been chosen to be the transverse phonon frequency at the X point to reproduce accurately the lattice vibrations where the density of states is larger. The effect of this choice on the elastic constants and on other frequencies is shown in Table 4.

In the following three Subsections, the analytic forms used and the details of the fit procedure are discussed for each of the three functions ϕ, ρ and U. It should be kept

Quantity	Experimental	Glue Model
B	1.803	1.803
C_{11}	2.016	2.203
C_{12}	1.697	1.603
C_{44}	0.454	0.600
$\nu_L(X)$	4.61	3.89
$\nu_T(X)$	2.75	2.75
$\nu_\pi(W)$	3.63	3.37
$\nu_\Lambda(W)$	2.63	2.75
$\nu_L(L)$	4.70	3.89
$\nu_T(L)$	1.86	1.94

Table 4

Experimental bulk modulus B, elastic constants (in 10^{12} dyne/cm^2, from ref. [53]) and phonon frequencies at points X,W and L of the Brillouin zone (in THz, from ref. [54]) compared with the values given by a glue hamiltonian fitted on B and $\nu_T(X)$.

in mind that these details can generally be dependent on the material which we are trying to reproduce, so that different materials may require a different procedure and/or different analytic forms.

2.8.1. Construction of the pair potential

The following analytical form has been used for $\phi(r)$:

$$\phi(r) = \begin{cases} a_4^I x^4 + a_3^I x^3 + a_2^I x^2 + a_1^I x + a_0^I & r<d \\ a_6^{II} x^6 + a_5^{II} x^5 + a_4^{II} x^4 + a_3^{II} x^3 + a_2^{II} x^2 + a_1^{II} x + a_0^{II} & d \leqslant r < r_c \\ 0 & r_c \leqslant r \end{cases}$$

where

$$x = r - d$$

and d is the first neighbours distance.

d	0.28782074421417 23E+01
r_c	0.37000000000000000E+01
ϕ_o	-0.80000000000000000E-01
a_0^I	-0.80000000000000000E-01
a_1^I	0.00000000000000000E+00
a_2^I	0.7619231375231362E+00
a_3^I	-0.8333333333333333E+00
a_4^I	-0.1211483464993159E+00
a_0^{II}	-0.80000000000000000E-01
a_1^{II}	0.00000000000000000E+00
a_2^{II}	0.7619231375231362E+00
a_3^{II}	-0.8333333333333333E+00
a_4^{II}	-0.1096009851140349E+01
a_5^{II}	0.2158417178555998E+01
a_6^{II}	-0.9128915709636862E+00

Table 5

Coefficients for $\phi(r)$ (gold fit).

The 12 coefficients are determined by the following conditions:

$\phi(d) = \phi_0$ (supplied)

$\phi'(d) = 0$ (lattice parameter, eq. (21))

$\phi''(d) = M\omega_T^2(X)/4$ (transverse phonons. eq. (29))

$\phi'''(d) = \phi'''_d$ (supplied)

$\phi(r^*) = 1$ eV (supplied)

$\phi(r_c) = 0$ (going to zero smoothly at $r=r_c$)

$\phi'(r_c) = 0$ (" " " " " ")

$\phi''(r_c) = 0$ (" " " " " ")

$\phi(r)$ continuous in r=d

$\phi'(r)$ " " "

$\phi''(r)$ " " "

$\phi'''(r)$ " " "

Four parameters are supplied externally: ϕ_0, r_c, r^* and ϕ'''_d. ϕ_0 is the depth of the potential, which (in the bulk gauge) determines the partition of the cohesion between the two-body part and the glue part. It also determines, to some extent, the anharmonicity of the potential: due to the first-neighbours constraint, a deep potential is more harmonic than a shallow one. This has visible effects, for instance, in the thermal expansion coefficient. Once ϕ_0 has been fixed, there is a very narrow range of possible values for r_c if wild oscillations of the derivatives of $\phi(r)$ are to be avoided. The last two parameters control the shape of the core region, which has a deep influence on melting and on surface properties. This point is discussed further in Subsection 2.8.3.

The parameters found for gold are given in Table 5, and the corresponding $\phi(r)$ is shown on Fig. 1.

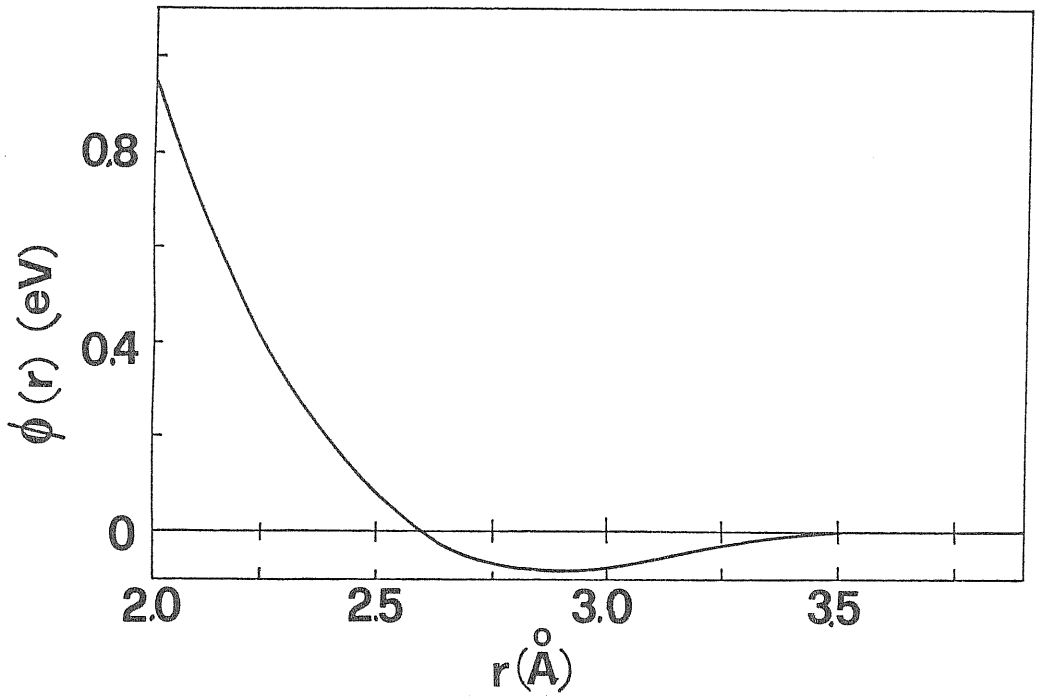

Figure 1. The pair potential $\phi(r)$.

2.8.2. Construction of the density function

The following analytical form has been used for $\rho(r)$:

$$\rho(r) = \begin{cases} b_3^I (r-d)^3 + b_2^I (r-d)^2 + b_1^I (r-d) + b_o^I & r<d \\ b_3^{II} (r-d)^3 + b_2^{II} (r-d)^2 + b_1^{II} (r-d) + b_o^{II} & d\leqslant r<r_b \\ b_3^{III} (r-r_m)^3 + b_2^{III} (r-r_m)^2 + b_1^{III} (r-r_m) + b_o^{III} & r_b\leqslant r<r_m \\ 0 & r_m\leqslant r \end{cases}$$

where d is the first neighbours distance.

The 12 coefficients are determined by the following conditions:

d	0.2878207442141723E+01
r_b	0.3500000000000000E+01
r_m	0.3900000000000000E+01
b_0^{I}	0.1000000000000000E+01
b_1^{I}	-0.6800000000000000E+00
b_2^{I}	0.7500000000000000E+00
b_3^{I}	-0.1333333333333333E+01
b_0^{II}	0.1000000000000000E+01
b_1^{II}	-0.6800000000000000E+00
b_2^{II}	0.7500000000000000E+00
b_3^{II}	-0.1527241171296038E+01
b_0^{III}	0.0000000000000000E+00
b_1^{III}	0.0000000000000000E+00
b_2^{III}	0.5578188675490974E+01
b_3^{III}	0.6132971688727435E+01

Table 6

Coefficients for $\rho(r)$ (gold fit).

$\rho(d) = 1$ (normalization, eq. (12))

$\rho'(d) = \rho_d'$ (supplied)

$\rho''(d) = \rho_d''$ (supplied)

$\rho'''(d) = \rho_d'''$ $(r<d)$ (supplied)

$\rho(r_b) = \rho_b$ (supplied)

$\rho(r_m) = 0$ (going to zero smoothly at $r=r_m$)

$\rho'(r_m) = 0$ (" " " " " ")

$\rho(r)$ continuous in $r=d$

$\rho'(r)$ " " "

$\rho''(r)$ " " "

$\rho(r)$ " " $r=r_b$

$\rho'(r)$ " " "

Here, six parameters are supplied externally: r_m, r_b, ρ_b, ρ_d', ρ_d'', and ρ_d'''. This leaves a great freedom in

determining the shape of this function.

It is worthwhile to note that $\rho(r)$ itself cannot fit any physical property, since it operates "within" U(n) in the hamiltonian. Only suitable combinations of $\rho(r)$ and U(n) are related to quantities of the physical system. One of such combinations is eq. (26) for the bulk modulus. From this equation, it is seen that the choice of ρ_d' is quite important, because fitting the bulk modulus then forces a particular value for U"(12), ϕ"(d) being fixed by the transverse phonons. This value for U"(12) may result to be incompatible with the general behavior of U(n), which is governed by other considerations such as the surface energy. Actually, the inverse route has been followed: first, a reasonable value for U"(12) is selected, then ρ_d' is determined by fitting the bulk modulus. This requires a sort of self-consistency in the fitting process, since U(n), as explained in the next Subsection, must be constructed after $\rho(r)$, and only at this last stage it is apparent whether the original choice for U"(12) was really good or not. A valid, if qualitative, quality test is the smoothness of U'(n) and U"(n), i.e. they should be free from spurious oscillations.

The value for ρ_d' resulting from this procedure gives a rather flat curve around r=d. The shape of $\rho(r)$ seen in Fig. 2 is the result of the competition between this small slope around r=3 Å and the short-range requirement. The "cutoff region" between r_b=3.5 Å and r_m=3.9 Å has been located in correspondence with the minimum between the first- and the second-neighbours shell in the pair correlation function (as determined by high temperature simulations). In this way, the effect of this region on the properties of the system has been reduced to a minimum.

The control provided by the two parameters ρ_d'' and ρ_d''' permits to adjust the shape of $\rho(r)$ in the very important region around r=d, which determines how the atoms gain and

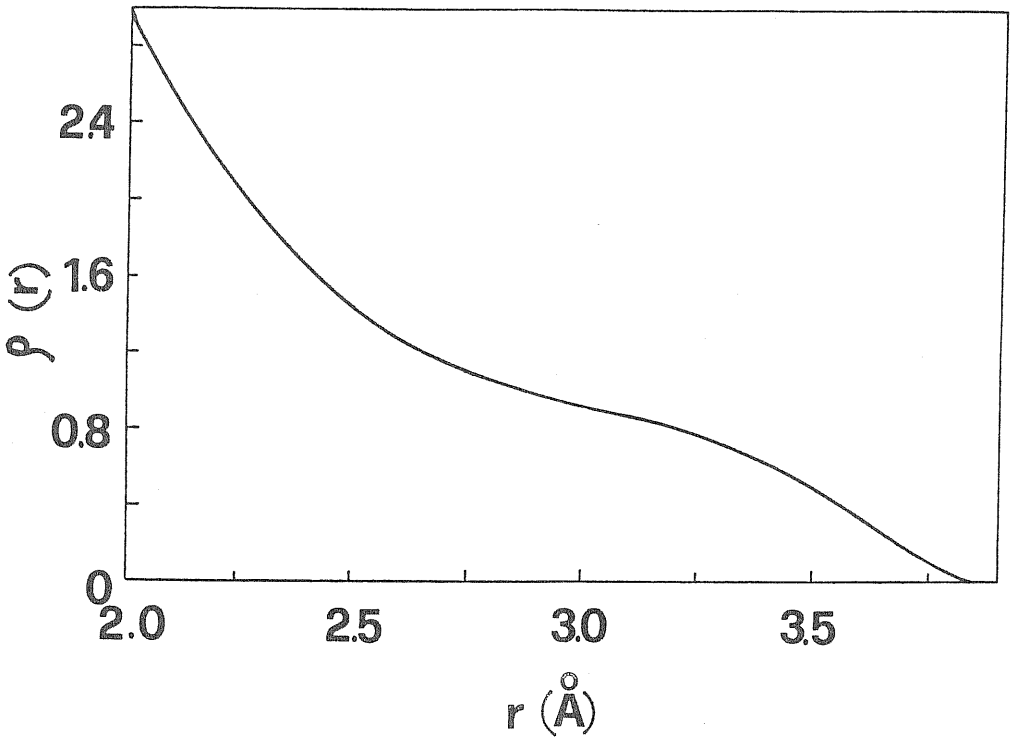

Figure 2. The density function $\rho(r)$.

lose coordination when their mutual distances are varied. Since the energies associated with coordination changes are large, slight modifications on $\rho(r)$ around the first neighbours distance can easily induce dramatic changes in the thermal behavior and in the surface properties. For example, the presence of surface reconstructions can be switched on or off by acting on $\rho(r)$ for $r<d$.

The parameters found for gold are given in Table 6, and the corresponding $\rho(r)$ is shown on Fig. 2.

2.8.3. Construction of the glue function

The following analytical form has been used for U(n):

$$U(n) = \begin{cases} c_4^I (n-n_s)^4 + c_3^I (n-n_s)^3 + c_2^I (n-n_s)^2 + c_1^I (n-n_s) + c_0^I & n<n_s \\ c_4^{II} (n-n_o)^4 + c_3^{II} (n-n_o)^3 + c_2^{II} (n-n_o)^2 + c_1^{II} (n-n_o) + c_0^{II} & n_s \leqslant n<n_o \\ c_3^{III} (n-n_o)^3 + c_2^{III} (n-n_o)^2 + c_1^{III} (n-n_o) + c_0^{III} & n \geqslant n_o \end{cases}$$

where n_o=12 (bulk coordination), and n_s is the first layer coordination on a relaxed (111) surface (defined below).

The 14 coefficients are determined by the following conditions:

n_o	0.120000000000000E+02
n_s	0.9358157767784574E+01
c_0^I	-0.2793388616771698E+01
c_1^I	-0.3420000000000000E+00
c_2^I	0.3902327808424106E-01
c_3^I	0.7558829951858879E-02
c_4^I	0.3090472511796849E-03
c_0^{II}	-0.3300000000000000E+01
c_1^{II}	0.0000000000000000E+00
c_2^{II}	0.8618226772941980E-01
c_3^{II}	0.4341701445034724E-02
c_4^{II}	-0.3044398779375916E-03
c_0^{III}	-0.3300000000000000E+01
c_1^{III}	0.0000000000000000E+00
c_2^{III}	0.8618226772941980E-01
c_3^{III}	0.4325981467602070E-02

Table 7

Coefficients for U(n) (gold fit).

$U(0) = 0$ (by definition, eq. (7))

$U(12) = U$ (cohesive energy, eq. (22))

$U'(12) = 0$ (bulk gauge, eq. (20))

$U''(12) = U_o''$ (bulk modulus, eq. (26))

$U(n^*) = 0$ (supplied)

$U(n_s) = U_s$ (surface energy, eq. (36))

$U'(n_s) = U_s'$ (supplied)

$U(n)$ continuous in $n=12$

$U'(n)$ " " "

$U''(n)$ " " "

$U(n)$ " " $n=n_s$

$U'(n)$ " " "

$U''(n)$ " " "

$U'''(n)$ " " "

Here, only two parameters are supplied externally: n^* and U_s'. n^* is greater than 12 and controls the shape of $U(n)$ for large coordinations. For gold, the value chosen ($n^*=17.48$) is such that the glue function rises rather rapidly above $n=12$. This rise corresponds to a sort of core-core repulsion, but obtained through the glue term instead of the two-body term. This peculiar behavior solves the following problem. In order to obtain a system with the correct melting temperature, the core region of the two-body potential should be soft enough to allow large vibrational amplitudes of the atoms. Such a "soft" system, however, would not be enough anharmonic to yield a realistic thermal expansion. A potential with a hard core region, on the other hand, gives a system which expands well but is too stiff and melts at a temperature which is too high. In the gold realization described here, the potential is soft and the anharmonicity is supplied by the glue: at high temperatures, in fact, the shape of the glue around $n=12$ favours fluctuations which tend to decrease, rather than increase, the local coordination. The system reacts by increasing

slightly the lattice parameter. Surface reconstructions involving large atom rearrangements are also favoured by soft two-body potentials [74].

The surface energy fit also deserves some comments. Once $\phi(r)$ has been assigned, U(12) is known by fitting the cohesive energy (eq. (22)) and at this point U(9) can be calculated using the expression (35) for the surface energy of a (111) face. However, this expression refers to an unrelaxed surface; relaxations raise the first layer coordination above 9, thus reducing the effective surface energy. To avoid this problem, a more sophisticated fitting procedure must be adopted. Assuming that only the distance between the first and the second layer is varied from the unrelaxed value $s_o = \sqrt{2/3}\ d$ to a certain value s, the expression for the surface energy per atom can be generalized as follows:

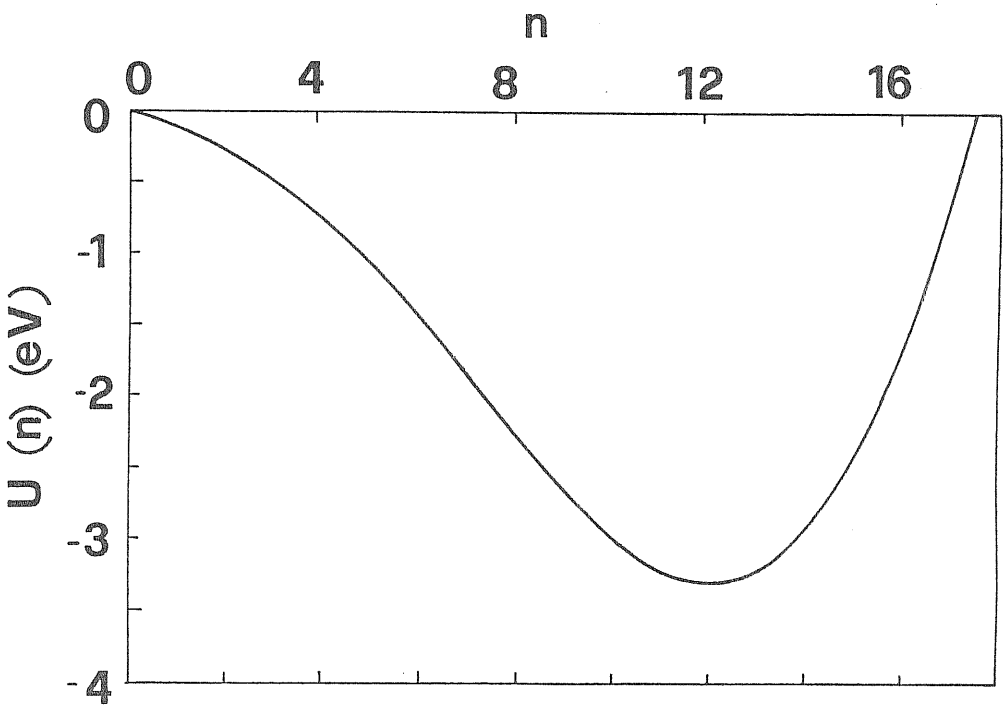

Figure 3. The glue function U(n).

$$E_S(s) = -\frac{9}{2}\phi(d) + \frac{6}{2}\phi(d') + \frac{6}{2}\phi(a') + U(n_S) + U(n_2) - 2U(12) \tag{36}$$

where d is the bulk first neighbours distance, $d'=\sqrt{s^2+d^2/3}$ the distance between an atom in the first layer and a first neighbour in the second layer, $a'=\sqrt{s^2+4d^2/3}$ the distance between an atom in the first layer and a second neighbour in the second layer, $n_S=6\rho(d)+3\rho(d')+3\rho(a')$ the first layer coordination, and $n_2=9\rho(d)+3\rho(d')+3\rho(a')$ the second layer coordination. Some second neighbours terms are present because, due to a possible contraction, it is not guaranteed that a' is larger than the range of $\phi(r)$ or $\rho(r)$. (36) is more complicated than (35), but can be straightforwardly calculated for a given value of s.

Our fitting procedure self-consistently solves the two equations

$$\begin{aligned} E_S(s) &= \sigma A \\ E_S'(s) &= 0 \end{aligned} \tag{37}$$

where σ is the experimental surface energy per unit area and $A=d^2\sqrt{3}/2$ is the area occupied by an atom. Equations (37) ensure that the correct surface energy is obtained in correspondence with the equilibrium relaxation. They are solved by using the following iterative method:

1. Build the region of U(n) with n>12; this can be done from the initial conditions, and will be never changed.
2. Assume an initial value for s.
3. Given s, calculate d', a', n_S and n_2.
4. Solve (36) for $U(n_S)$. Note that $U(n_2)$ is known, since $n_2>12$. This gives the condition $U(n_S)=U_S$.

5. Now all the coefficients of U(n) can be determined, so that U(n) becomes known for all n's.

6. Solve $E_S'(s)=0$. This yields a solution $s' \neq s$.

7. If $|s-s'|<\varepsilon_S$ and $|E_s(s)-E_s(s')|<\varepsilon_E$ (where ε_S and ε_E are very small tolerances) then terminate, otherwise rename s' as s and go back to step 3.

Note that the final shape for U(n) is controlled by the parameter U_S' which is supplied externally. If a reasonable value is given to this parameter, the procedure converges within ten iterations. Relaxation effects between the second and the third layer and between deeper layers, neglected by this method, lead to a very small (-0.2%) correction, as a molecular dynamics calculation established later. This correction is surely negligible in comparison with the error associated with the experimental estimate of the surface energy [52].

The parameters found for gold are given in Table 7, and the corresponding U(n) is shown on Fig. 3.

CHAPTER III
MOLECULAR DYNAMICS STUDIES OF BULK PROPERTIES

3.1. Fcc stability and thermal expansion

The bulk thermal properties of the system have been studied using the Parrinello-Rahman molecular dynamics technique [56]. In this method, the box containing the particles (and extended to infinity through periodic boundary conditions) can vary in volume and shape, under the action of internal stresses and, if present, an externally applied pressure or anisotropic stresses. It has been shown [56] that changes in the shape of the box allow the (previously impossible) observation by molecular dynamics of solid-solid transformations, such as that of an fcc crystal into a bcc and viceversa. These phase transformations can be induced by applying external forces, but they may also occur spontaneously if at a certain temperature the two phases have the same free energy [57].

The stability of the fcc structure of gold (as described by the glue hamiltonian) against the bcc structure [*] has been therefore verified up to the melting temperature through Parrinello-Rahman simulations in the absence of pressure or stress.

The variation of the lattice parameter with the temperature, shown on Fig. 4, is in excellent agreement with the experimental data [58]. It should be noted that the thermal expansion curve is one of the quantities fitted in the generalized sense discussed in Sec. 2.7.

---

[*] The fcc-hcp stability is more delicate, because it involves atom displacements relative to the box, as well as variations in the box shape [56]. No conclusion can be drawn about this point. Note that at T=0, with the glue hamiltonian, the fcc is favoured over the bcc, while fcc and hcp have the same energy.

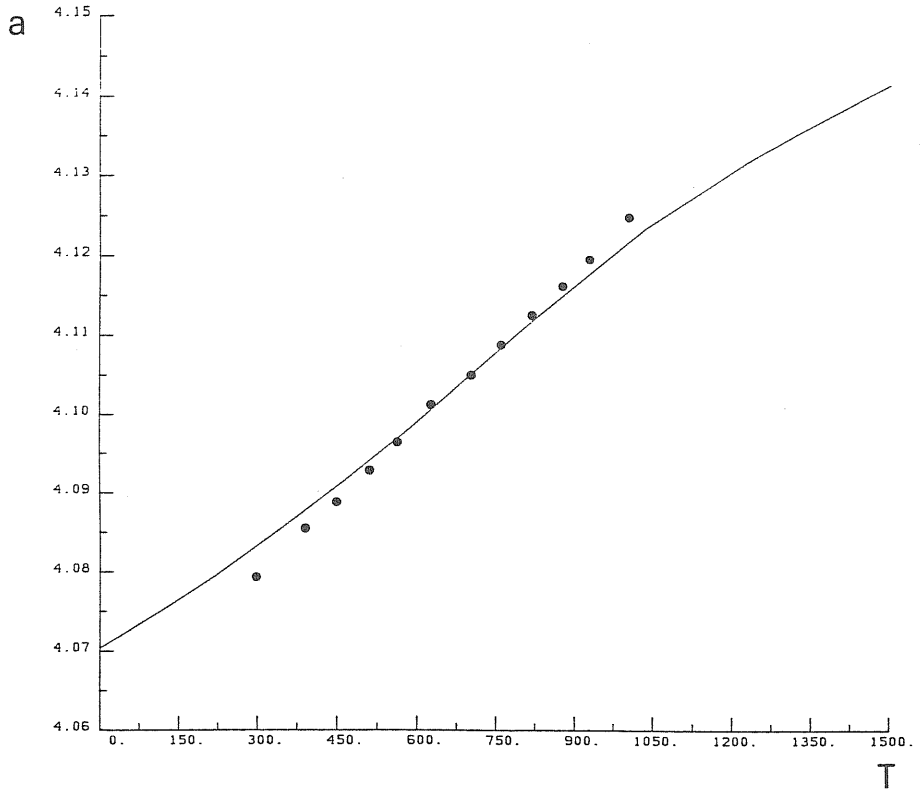

Figure 4. Lattice parameter a as a function of the temperature. The solid line is the result of the simulation; the dots are the experimental data [58].

3.2. Melting point

The melting temperature has been determined by computer simulation [59]. A bulk simulation is not well suited for this purpose because, lacking any defects, it undergoes overheating and supercooling, i.e. it exhibits a large hysteresis effect which makes it difficult to locate even approximately the melting point [60]. A system with a free surface overcomes this problem, because the melt can easily nucleate at or near the surface and then propagate into the bulk [61,22,23].

In order to determine the melting temperature, the following procedure has been followed. A system with a free surface is heated until a spontaneous nucleation of the liquid phase occurs at the surface. The system is then kept hot, to allow for the motion of the liquid-solid interface into the bulk. In this way we produce a sample with a

liquid phase and a solid phase simultaneously present, although not in perfect equilibrium. Starting from this sample, the melting temperature, at which by definition the liquid-solid interface remains stationary, is searched by trial-and-error.

The melting temperature is a function of the pressure or, more generally, of the stress applied on the system. We have kept the stress equal to zero by adjusting the lattice parameter of the crystalline phase to match the value obtained by the thermal expansion curve at each temperature. This is done by scaling of the molecular dynamics cell. The liquid is not under pressure due to the presence of the free surface.

The resulting value for the melting temperature is

$$T_m = 1357 \pm 5\,^{\circ}K$$

At T=1350 °K, we observe a motion of the liquid-solid interface in the direction of the solid, eventually leading to a complete recrystallization of the sample; at T=1360 °K, on the other hand, the melt is seen to proceed into the bulk. The estimate of the melting temperature is based on the different interface velocities observed at these two temperatures. The value obtained for T_m is in good agreement with the experimental datum, T_m^{exp}=1336 °K.

We have also estimated the latent heat of fusion by comparing the average energy per particle in the liquid and in the solid phase. The result is

$$\Delta H_m = 0.115 \pm 0.005 \text{ eV/atom}$$

The entropy change on fusion is therefore

$$S_m = \Delta H_m / T_m = 0.98 \pm 0.05 \; k_B/\text{atom}$$

These values are only slightly lower than the experimental values (see Table 1), which is very satisfactory.

The volume change on melting has also been estimated. In this case, the value obtained (0.6%) is one order of magnitude smaller than the experimental value (5.2%, from Table 1). We can attribute this discrepancy tentatively to the extreme softness of the core of our two-body potential. This feature is however essential in producing the extreme "ductility" of our model system, which allows among other things all rearrangements to occur in a reasonably short time in terms of a molecular dynamics simulation.

At the time of writing, a detailed study of the melting transition is in progress [59].

3.3. Liquid structure

The pair correlation function g(r) of the liquid predicted by the glue hamiltonian has been calculated using molecular dynamics. The box used in the simulation contains 500 particles and is extended to infinity in all the directions by periodic boundary conditions. The conditions assumed are zero pressure and a temperature of 1600°K.

Starting from a crystalline state, the system is brought at T=2000°K in order to melt quickly. After 3000 steps of equilibration, the temperature is decreased to 1600°K, and the system is equilibrated again for 3000 steps. The pair correlation function has been measured in the subsequent 1000 steps; the result is shown on Fig. 5, compared with the experimental g(r) at T=1573°K [62]. There is a substantial agreement on the position, height and width of the first peak. The calculated g(r) has, however, the first minimum too deep, and the second shell slightly too close when compared with the experimental g(r).

From the same calculation, the self-diffusion coefficient has also been extracted by using the relation [63]

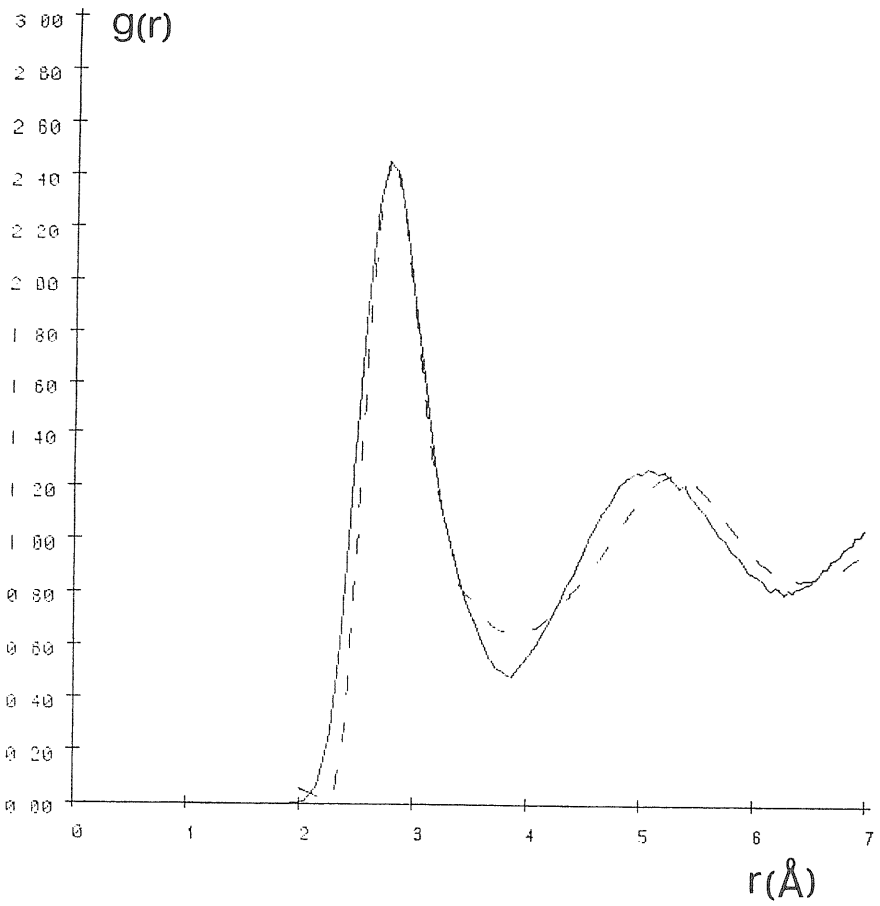

Figure 5. Calculated (solid line) and experimental (dashed line) [62] pair correlation function g(r) of liquid gold.

$$\langle |\vec{r}(t) - \vec{r}(0)|^2 \rangle = 6Dt$$

The resulting value (averaged on the 500 atoms) is $D=2.2\cdot10^{-5}$ cm^2/sec. Unfortunately, no experimental values have been found in literature for liquid gold.

As a final observation, it may be noted from g(r) that the distance between a pair of particles, in practice, is always larger than 2 Å; in this simulation it is also seen that the distribution of the coordinations n (in the glue hamiltonian sense) of the atoms is confined in the interval 9-14 (with an average value of 11.6). At surfaces, the

lower bound of the coordination distribution decreases to about 7. As discussed at the end of Sec. 2.7, these values indicate the limits of validity for the functions in the glue hamiltonian: we do not expect that modifications made to these functions out of the ranges sampled in simulations would yield visible effects on the properties of the system. The validity range can be thus summarized: $r>2$ Å, $7<n<14$.

3.4. Vacancy formation

As already stated in Sec 1.2, the vacancy formation energy is given by

$$E_V = E_N^* - E_N$$

where E_N is the energy of a system with N particles in N perfect crystal sites, while E_N^* is the energy of a system with N particles in N+1 crystal sites, that is, when a vacancy is present. In the same terms we can define the vacancy formation volume:

$$\Omega_V = \Omega_N^* - \Omega_N$$

Neglecting relaxations, the formation energy predicted by the glue hamiltonian can be calculated using eq. (34). This gives

$$E_V^{(o)} = 1.458 \text{ eV}$$

which is about 50% higher than the experimental value, $E_V^{exp} = 0.95$ eV [10]. Atom relaxations around the vacancy, however, reduce the formation energy.

Relaxations effects have been included by using molecular dynamics. The procedure consists in performing a simulated quenching, where the atoms are moved accordingly to the instantaneous forces but their velocities are rescaled

by a factor $\alpha<1$ at every time step of the simulation. In this way, kinetic energy is continuously removed until the system eventually reaches a stationary state where all the atoms are at rest in their relaxed equilibrium positions and the energy is minimized.

A problem lies in the fact that a point defect in a crystal generates an elastic strain which at large distances falls as $1/r^3$ [64]; but in molecular dynamics calculations the range of the distortion is limited by the size of the computational box (subjected to the usual periodic boundary conditions), so that long-range contributions are lost. However, these contributions can be estimated by noting that the density of elastic energy w(r) at a distance r from the defect decays like $1/r^6$ (the square of the strain). Therefore, the total elastic energy W(R) associated to deformations at distances r>R falls, for large R, as

$$W(R) \cong \int_R^\infty 4\pi r^2 w(r) dr \sim \frac{1}{R^3}$$

For this reason, we expect that vacancy formation energy calculations performed on a cubic box of size La (where a is the lattice parameter) should exhibit a dependence on L of the kind

$$E_v(L) \cong \bar{E}_v + \frac{A}{L^3} \qquad (38)$$

By fitting this relation to the values of $E_v(L)$ extracted from the simulations, the asymptotic term $\bar{E}_v$ can be estimated.

Two sets of calculations have been performed, with L=3,4,5,6, and $N=4L^3-1=107,255,499,863$.

Set a)

In this set, the volume of the box is kept fixed accordingly to the T=0 lattice spacing of the perfect

crystal. This corresponds to imposing a vacancy formation volume equal to the atomic volume Ω_o. The resulting energies are given in the second column of Table 8, while in the third column these energies have been fitted by eq. (38), with $\bar{E}_v$=1.2624 eV and A=+1.0482 eV.

Set b)

In this set, the volume of the box is allowed to vary in order to compensate the internal pressure induced by the vacancy. In this case, the vacancy formation volume becomes less than Ω_o and can be measured. The results are given in Table 9. The fit parameters in eq. (38) are $\bar{E}_v$=1.2620 eV and A=-0.6404 eV.

Set a) calculations overestimate the formation energy, while set b) calculations underestimate it. The explanation lies probably in the fact that in set b), the attractive interaction between the vacancy and the other image

L	E_v	eq.(38)
3	1.3013	1.3012
4	1.2787	1.2788
5	1.2705	1.2708
6	1.2676	1.2673

Table 8

Vacancy formation energies E_v (in eV) from constant volume calculations, and best fit from eq. (38).

L	E_v	eq.(38)	$\Delta a/a_o$	Ω_v/Ω_o
3	1.2383	1.2383	-0.27	0.1408
4	1.2518	1.2520	-0.11	0.1459
5	1.2567	1.2569	-0.06	0.1476
6	1.2592	1.2590	-0.03	0.1484

Table 9

Vacancy formation energies E_v (in eV) from zero pressure calculations, best fit from eq. (38), corresponding lattice parameter variation $\Delta a/a_o$ (in %) and vacancy formation volume in atomic volume units.

vacancies in the nearby computational boxes is stronger than in set a), where it is almost nullified by the constant volume constraint. The two sets are in remarkable agreement for the value of $\bar{E}_V$. Dropping the last digit, we can thus assume

$$E_V = 1.262 \text{ eV}$$

as the vacancy formation energy predicted by the glue hamiltonian and, from set b),

$$\Omega_V = 0.15\,\Omega_o$$

as the vacancy formation volume, which is only weakly dependent on the box size. This value appears to be low compared with the experimental datum, $\Omega_V^{exp}=0.5\Omega_o$ [65].

Finally, the relaxations of the first four atomic shells around the vacancy in the case L=5 are given in Table 10, together with the atomic coordinations n (in the glue hamiltonian sense). It can be seen that all the four shells move towards the vacancy. It is interesting to note [66]

Shell	R	ΔR	n
Set a)			
1	2.8324	-0.0458	11.205
2	4.0205	-0.0499	12.109
3	4.9447	-0.0405	12.041
4	5.7255	-0.0309	12.009
Set b)			
1	2.8298	-0.0484	11.219
2	4.0184	-0.0520	12.123
3	4.9416	-0.0436	12.055
4	5.7220	-0.0344	12.022

Table 10

Distance R from the vacancy (in Å), relaxation ΔR respect to the unrelaxed distance (in Å) and coordination n for the first four atomic shells around the vacancy. Set a) is the constant volume calculation, set b) is the zero pressure calculation.

that in two-body systems with interactions not limited to the first neighbours, the first shell relaxes towards the vacancy but the other shells move away from it.

CHAPTER IV
Au(100) SURFACE RECONSTRUCTION

4.1. Au(100): experimental evidence

The (100) surface of gold has long been known to reconstruct [67-76]. It is by now well established that the reconstruction is characterized by a close-packed triangular overlayer on a square substrate. The first, low-resolution LEED measurements [67,68] indicated a (1x5) reconstruction cell. This pattern was interpreted as due to a geometry where six rows of atoms lie on top of five [011] rows of substrate atoms in a $[01\bar{1}]$ direction (henceforth direction y), while the registry with the substrate is preserved in the orthogonal [011] direction (henceforth direction x). This arrangement requires a 3.77% contraction of a perfect triangular lattice in the 6-onto-5 (y) direction. Later, LEED measurements with improved resolution [71] suggested (20x5) as a better unit cell for the reconstruction. This was interpreted to imply a small contraction also in the x direction, so as to accommodate one extra row over 20 $[01\bar{1}]$ substrate rows. Subsequently, LEED [74] and He-scattering [75] studies suggested a much larger unit cell such as c(26x68), as the result of the additional contraction in the y direction. In a recent scanning-tunneling-microscope (STM) real-space investigation [76], Binnig, Rohrer, Gerber and Stoll propose a $\begin{pmatrix} 26 & 0 \\ z & 48 \end{pmatrix}$ unit cell where $-5 \leqslant Z \leqslant 0$, implying an additional y contraction but also the possibility of a small rotation (about 0.1 degrees) of the whole overlayer over the substrate.

From the physical point of view, the most important feature of the Au(100) reconstruction is the close packing achieved by the topmost layer. This indicates the surface density increase as the driving force behind reconstruction. The energy of the system is lowered by this density increase, overcoming the strain energy cost caused by the

misfit between the square substrate and the triangular overlayer.

While plausible but speculative arguments have been advanced to justify such behavior, there exists as yet no detailed theoretical description of the phenomenon. At the "ab initio" microscopic level the task is certainly a very difficult one, due to the great complexity of the electronic problem [77]. On the other hand, the phenomenological scheme provided by the glue hamiltonian constitutes a useful tool to study surface reconstructions. The rise of U(n) for decreasing coordinations, such as one finds at a surface, provides a natural driving force for reconstruction: since the coordination of a surface atom is poor, it pays to reconstruct into a denser layer, with better coordination.

4.2. (1x5) reconstruction

An investigation of the Au(100) surface structure predicted by the glue hamiltonian has been carried out using molecular dynamics. This is done by studies of slabs with in-plane periodic boundary conditions and initially 5x5=25 atoms per (100) plane. The area of the slab and its square shape are kept rigid to prevent transformation into a (111) slab. The area is readjusted at each temperature to match the bulk thermal expansion, taken from the calculation described in Sec. 3.1. It is found that a number of layers L=14 is sufficient to decouple the two surfaces.

First of all, the energetics have been studied by using molecular dynamics mainly as a tool to generate the minimal energy configuration. The typical procedure consists of warming the slab up to about $T_m/2$ and, after equilibration, of gradually cooling back to T=0. The total length of the cycle is of the order of 10000 molecular dynamics steps (1 step = $7 \cdot 10^{-15}$ seconds). This method does not guarantee attainment of the absolute minimum. However, it is always possible to improve one's confidence in a given

configuration by trying different annealing schedules, and by starting from different initial conditions.

This procedure has been first applied to the clean, unreconstructed (100) faces. Figure 6(a) shows the appearance of the first atomic layer after annealing. One can note that the surface atoms have shrunken together, leading to formation of close-packed stripes (five atomic rows each) separated by a gap [*]. This gap in turn can be seen as leading to the formation of two monoatomic steps, here still very near to one another. The second layer has remained a basically perfect (100) plane. This is a clear indication that our (100) surface wants to reconstruct into a denser layer, even within the constraint of our small 5x5 cell.

To pursue further this idea, we have made a series of runs where a number n of extra adatoms is added on top of the first layer. n is varied throughout the range from n=1 to n=25. For n small, the extra atoms are absorbed into the first layer giving rise, after annealing, to a denser packing. At the same time, we find a decrease of surface energy, of surface energy, defined as

$$\sigma(n) = \frac{E(N)-NE_c}{2A}$$

where N=25L+2n is the total number of particles in the sample, E(N) the total energy of the slab, E_c the cohesive energy, A the surface area and the factor 2 accounts for two surfaces. A minimum of $\sigma(n)$ is obtained for n=5, as shown by Fig. 7. The corresponding first-layer arrangement of Fig. 6(b) is a good candidate for explaining the Au(100) reconstruction. The second and deeper layers retain a strained (100) character, in agreement with the experimental

---

[*] By a careful quench of a perfect crystal, not preceded by heating and thermal equilibration, a relaxed but perfect (100) surface has been indeed produced. Its surface energy, however, is higher than that of the configuration with the gaps (128.5 vs. 109.6 meV/Å^2).

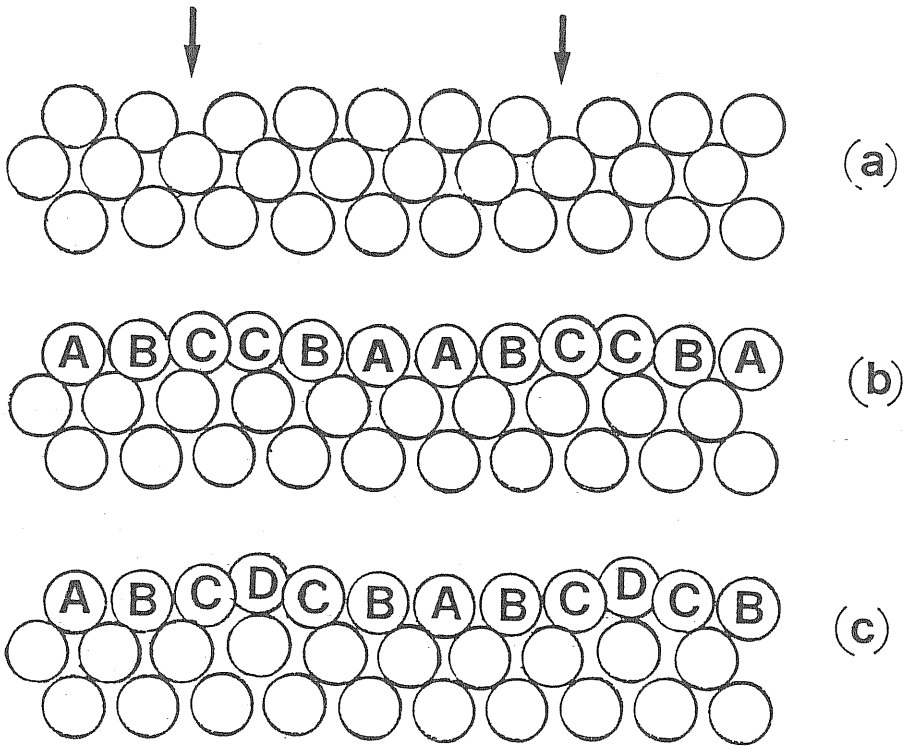

Figure 6. Side views of minimum energy configurations of (100) slabs after thermal equilibration and subsequent annealing. Two molecular dynamics cells are shown for clarity.

(a) The starting configuration was a perfect (100) slab. The atoms have shrunken in 5-rows wide stripes, leaving a gap (indicated by the arrow) in between. The surface energy is 109.6 meV/Å^2.

(b) 5 additional adatoms present in the starting configuration. They are absorbed, giving rise to a 20% denser quasi-triangular reconstructed first layer with a ABCCBA stacking. The surface energy is 102.3 meV/Å^2.

(c) Same as (b), but the registry is different and the stacking is ABCDCB. The surface energy is 102.6 meV/Å^2.

All atomic positions shown to scale (not schematic), but atom radii are arbitrary. Vertical (z) direction [100], horizontal (y) direction [011].

findings [72]. The amplitudes of the corrugation predicted for the first 4 layers are ξ_1=0.47 Å, ξ_2=0.21 Å, ξ_3=0.13 Å, ξ_4=0.08 Å. The relaxations of the distances between average layer positions are Δd_{12}=+3.6%, Δd_{23}=+2.2%, Δd_{34}=-0.2%. The increase of d_{12} and d_{23} is due to excessive coordination in the second layer, caused by the first-layer reconstruction. The stacking of the rows is ABCCBA, as on Fig. 6(b). A local energy minimum has been also found at another stacking ABCDCB, shown in Fig. 6(c). In this arrangement the surface energy is slightly higher and the corrugation is larger (ξ_1=0.74 Å). In all cases the strain is not uniformly distributed: the surface density is higher in a hilltop row, and lower in a valley row, where the atoms are not far from their ideal hollow-site positions over the square substrate.

Of course the role played by the cell size in these calculations is not a minor one. The n=5 "best" configuration has a (1x5) reconstructed structure which fits very well in our 5x5 cell. On the other hand, the use of different cells may reveal the existence of reconstructed surfaces with a still lower surface energy. Following this idea, calculations of the same kind have been performed, with cells suited to the following reconstruction patterns: (1x7), (1x12), (1x8), (1x3), respectively of the kind 8-onto-7, 14-onto-12, 10-onto-8, 4-onto-3 (in increasing order of surface density). All these surfaces reconstruct into a denser overlayer, and the surface energies are (in the order) 103.7, 103.2, 103.3, 108.6 meV/Å^2 [*]. Since they are all higher than the (1x5) surface energy (102.3 meV/Å^2 for the ABCCBA registry or 102.6 meV/Å^2 for the ABCDCB registry), the (1x5) is the preferred pattern.

---

[*] Of course, the absolute level of confidence on the energetic accuracy of the glue scheme is far from the level of the meV per atom. The accuracy of relative energy differences, however, can be very different, and should basically be as good as the physical description behind the hamiltonian. In this sense, it is meaningful to seek the optimal configuration, even among possibilities which are energetically very close.

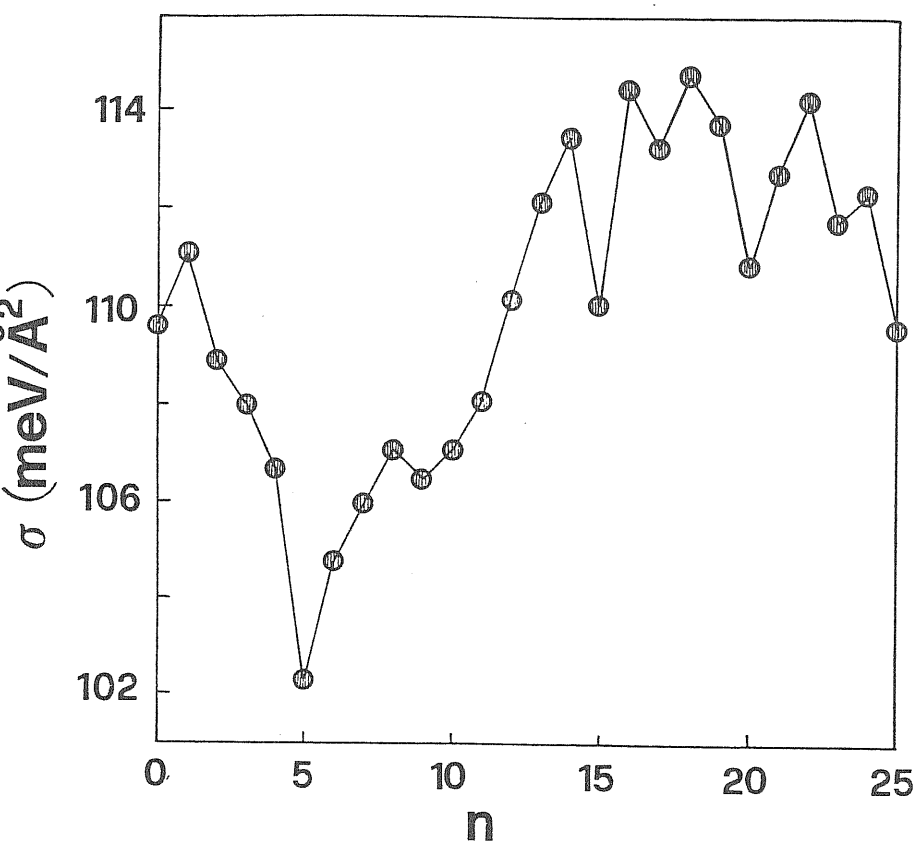

Figure 7. Surface energy of the final configurations as a function of the number of adatoms present at the start in a (5x5) (100) slab. The minimum at n=5 corresponds to the configuration in fig. 6(b).

4.3. (34x5) ''solitonic'' reconstruction

So far we have considered only the reconstruction along the five-fold y [01$\bar{1}$] direction, which gives rise to the basic (1x5) pattern. In this geometry, the quasi-triangular overlayer is contracted on the average by 3.77% in the y direction while it is in registry with the underlying lattice in the x [011] direction. On the other hand, the unit cell has been regarded as a (20x5) for a long time [74], indicating a 4.76% average contraction along x. More recent STM measurements [76] suggest a more accurate (26x48)

structure, where the contractions are 3.83% along x and 4.42% along y.

The optimal contraction in the x direction at T=0 has been searched by studying the surface energies of reconstructed (Mx5) 12-layers slabs. No provision is made for an additional contraction in the y direction or a small overall rotation (both leading to much larger unit cells) and for finite temperature effects. The results are summarized in Fig. 8. This analysis leads to the following interesting

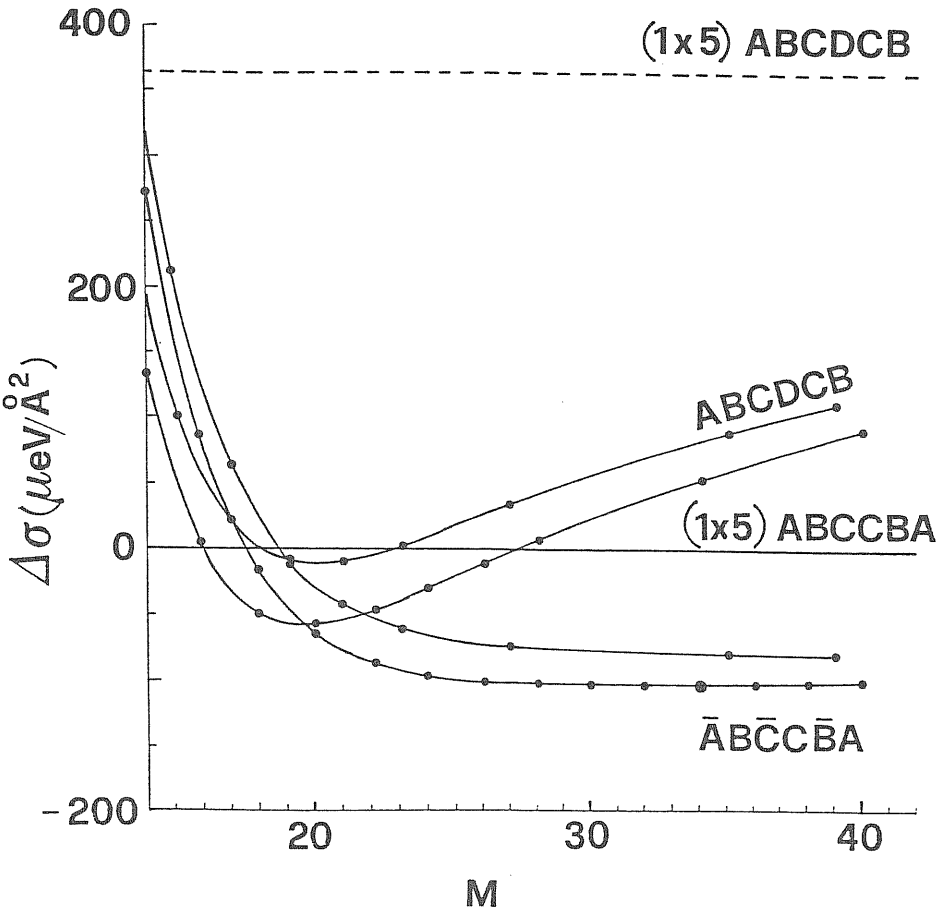

Figure 8. Differences of surface energies of (Mx5)-reconstructed slabs, respect to a (1x5)-reconstructed ABCCBA slab, as a function of M. The two basic y registries ($\bar{A}B\bar{C}C\bar{B}A$ and ABCDCB) show different behaviors. For each registry, the odd M case is slightly disfavoured. The optimal surface is $\bar{A}B\bar{C}C\bar{B}A$, M=34.

points:

(1) After annealing, some of the small distortions that take place break the exact mirror plane symmetry of ABCCBA. The relaxed surfaces have instead a lower symmetry of the type $\bar{A}B\bar{C}C\bar{B}A$, where A and $\bar{A}$, B and $\bar{B}$, C and $\bar{C}$ are different as discussed below.

(2) the $\bar{A}B\bar{C}C\bar{B}A$ arrangement provides the overall surface energy minimum, and leads to larger unit cells than ABCDCB.

(3) the best length M of the (Mx5) unit cell is M=34, but the minimum of the surface energy is so flat as to make this precise value almost meaningless: any value of M between 28 and 38 is about equally good. In particular, the surface energy of (34x5) is only 0.003% less than (26x5), which is a unit cell very close to the suggested experimental cell (26x48) [76]. This can be regarded as a pretty good agreement.

(4) the odd M cells cost more energy to realize than the even M cells. This has to do with the presence of a defect [78]. The defect-free situation is that of even M, which therefore must be taken as representative of the perfect surface.

Let us now consider the structural features of the optimal (100) surface arrangement, i.e. $\bar{A}B\bar{C}C\bar{B}A$, (34x5), as resulting from the molecular dynamics minimization. A more detailed discussion can be found in ref. [79]. Fig. 9(a) shows a perspective view of the first three layers of this slab. The contraction along x induced by the density increase is not uniform but localized in soliton-type regions [80], stacked to give rise to a slightly distorted centered rectangular superlattice. In correspondence with the soliton centers, the corrugation in the y direction has a double-maximum-double-minimum structure (due to the alter-

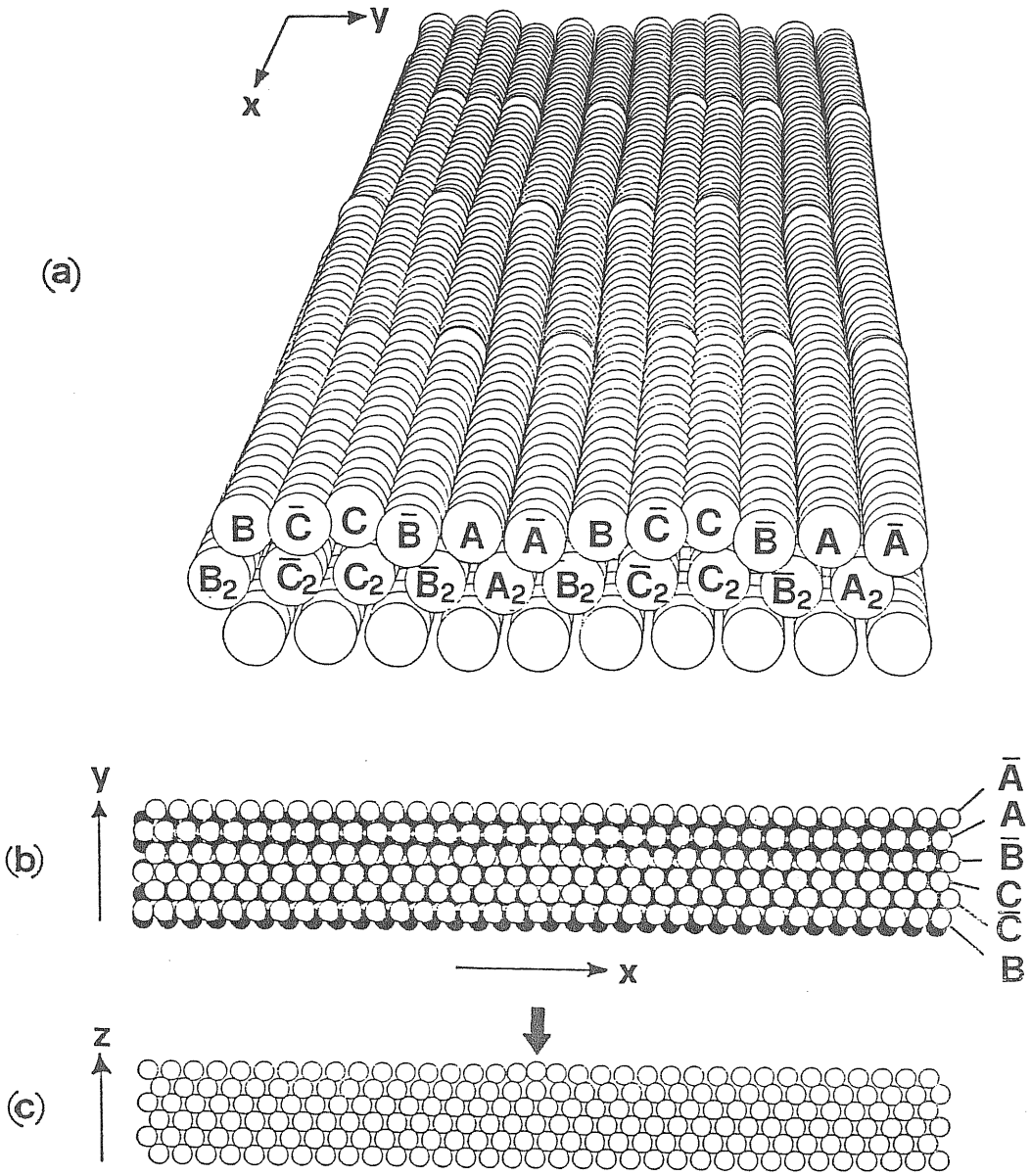

Figure 9: The optimal $\bar{A}B\bar{C}C\bar{B}A$ (34x5) surface. The surface energy is 102.2 meV/Å^2.

(a) Perspective view showing the soliton lattice. A 2x2 array of cells is shown.

(b) Top view of the first (white atoms) and the second layer (black atoms).

(c) Side view of the first six layers. The first layer (a $\bar{B}$ row is shown) has a soliton in the middle.

nating stacking of solitons) and is large (0.8 Å). In the middle of the regions between the solitons, the corrugation and the overall structure are very similar to the ABCCBA (1x5) cell. Here, the y-corrugation is 0.5 Å, single-maximum-single-minimum. This corrugation coincides numerically with the value suggested by the He-scattering analysis of Rieder et al. [75]. The solitons slightly compress the surface atoms in these middle regions. The resulting glue energy gain more than compensates the formation energy of the solitons. Also the multilayer relaxations, generally close to those of the (1x5) above, become soliton-modulated.

The detailed discussion provided by Binnig, Rohrer, Gerber and Stoll of the Au(100) surface morphology obtained by STM allows some further comparison with our calculated structure. Their STM micrograph, shown on Fig. 10, exhibits an alternation of "smooth ribbons" with "rough ribbons". In the former, the corrugation is single-minimum-single-maximum with an amplitude of ~0.5 Å [81], while in the latter the corrugation is double-maximum-double-minimum with a total amplitude of ~1 Å. We can identify the "rough ribbons" as the stripes joining solitons along $[01\bar{1}]$, and the "smooth ribbons" as the wide flat regions in between. The rough ribbons seem narrower in our calculation than in the STM picture. However, it is possible that this could be due to temperature smearing, rather than a genuine disagreement.

While differing in several ways from the hard-sphere model used in Ref. [76] to interpret the experimental results, the present structure seems generally more plausible, and no less compatible with the data. A more recent STM experiment [82] appears to confirm the correctness of this solitonic description.

In conclusion, it has been shown how an extremely detailed picture of the reconstructed Au(100) surface can be obtained by starting from the same glue hamiltonian which

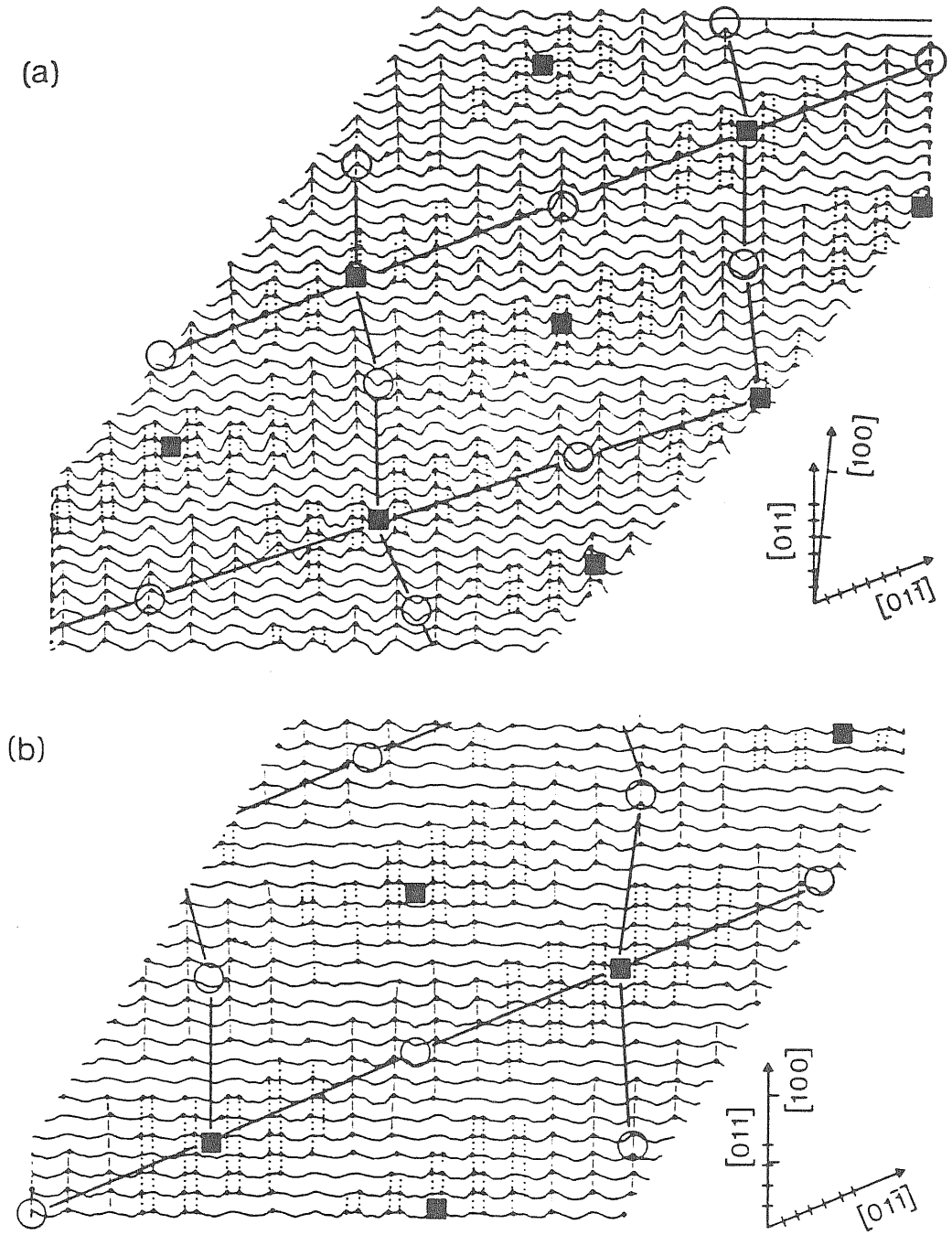

Figure 10. STM micrographs of Au(100), taken from ref. [76]. They show the alternating sequences of "rough ribbons", with a double-maximum-double-minimum corrugation pattern, and "smooth ribbons", with a single-maximum-single-minimum pattern. These ribbons are oriented along [011]. Division on the axes correspond to 5 Å. The bold lines show the unit cell, ~(26x48). [011] is direction x and [01$\bar{1}$] direction y in Figure 9.

reproduces the bulk properties. The resulting energetics and surface atomic arrangement appear realistic, and compare favourably with known experimental facts.

CHAPTER V
CONCLUSIONS AND OUTLOOK

The glue hamiltonian is a completely empirical way to represent atomic interactions in a metallic system. It constitutes a major step forward respect to standard two-body descriptions; in fact, all the main faults of pairwise forces are overcome without introducing a significant computational overhead.

This study has shown that a detailed picture of the Au(100) surface reconstruction can be achieved, together with a good description of bulk cohesive and thermal properties of gold. Moreover, the Au(110) "missing row" reconstruction [83] and the Au(111) reconstruction [84] are also well reproduced and characterized by the glue model. Therefore, the glue hamiltonian appears as an extremely useful tool to study the properties of metals by computer simulation in a realistic way.

Other studies presently planned or under way concern surface phonons on reconstructed Au(111) [85], the melting transition with particular attention to surface effects [59], melting and structural properties of small gold clusters [86], bulk defects, as well as extensions to other metals.

Acknowledgements

I wish to thank prof. Erio Tosatti and prof. Michele Parrinello for suggesting the glue idea and thoroughly supporting and keeping alive this project for over three years; Mario Garofalo for his nice analytical work on the glue hamiltonian and for endless discussions; Alvise Nobile and his staff for the enormous efforts spent to provide for a good computing environment among objective difficulties; professors Volker Heine and Heinrich Rohrer for useful discussions on the glue model and on surface reconstructions; Toni Schneider, Art Williams and the staff at the IBM Zurich Research Laboratory for their hospitality during the summer 1985 and the excellent computer resources they made available to me; and all the other people who have contributed ideas and helped to complete this project.

References

[1] see, e.g., J.M. Ziman, "Electrons and phonons" (Oxford University Press, 1960).

[2] R. Car and M. Parrinello, Phys.Rev.Lett. 55 (1985), 2471.

[3] J.A. Barker, in "Rare Gas Solids" Volume I, ed. by M.L. Klein and J.A. Venables (Academic, London, 1976).

[4] R. Taylor, Physica 131B (1985), 103, and references therein.

[5] C.S. Jayanthi, E. Tosatti and A. Fasolino, Phys.Rev. B 31 (1985), 470.

[6] C. Kittel, "Introduction to Solid State Physics", 3rd ed. (Wiley, New York, 1966).

[7] A.R. Ubbelohde, "The molten state of matter" (Wiley, Chichester, 1978).

[8] A.J.C. Ladd and L.V. Woodcock, Molec.Phys. 36 (1978), 611.

[9] A.V. Chadwick and H.R. Glyde, in "Rare Gas Solids" Volume II, ed. by M.L. Klein and J.A. Venables (Academic, London, 1977).

[10] A. van den Beukel, in "Vacancies and Interstitials in Metals", ed. by A. Seeger, D. Schumacher, W. Schilling and J. Diehl (North-Holland, Amsterdam, 1970), p. 427.

[11] R. Feder and A.S. Nowick, Phil.Mag. 15 (1967), 805.

[12] A. Seeger and H. Mehrer, in "Vacancies and Interstitials in Metals", ed. by A. Seeger, D. Schumacher, W. Schilling and J. Diehl (North-Holland, Amsterdam, 1970), p. 1.

[13] Ya.A. Kraftmakher and P.G. Strelkov, in "Vacancies and Interstitials in Metals", ed. by A. Seeger, D. Schumacher, W. Schilling and J. Diehl (North-Holland, Amsterdam, 1970), p. 59.

[14] M. Born and K. Huang, "Dynamical theory of crystal lattices" (Oxford University Press, Oxford, 1954), chapter III.

[15] H.B. Huntington, in Solid State Physics Volume 7, ed. by F. Seitz and D. Turnbull (Academic, New York, 1958).

[16] P. Korpiun and E. Luscher, in "Rare Gas Solids" Volume II, ed. by M.L. Klein and J.A. Venables (Academic, London, 1977).

[17] R. Benedek, J.Phys. F 8 (1978), 1119.

[18] R.P. Gupta, Phys.Rev. B 23 (1981), 6265.

[19] F. Jona, J.Phys. C 11 (1978), 4271.

[20] G. De Lorenzi and G. Jacucci, Surf.Sci. 164 (1985), 526.

[21] A. Fasolino, G. Santoro and E. Tosatti, Phys.Rev.Lett. 44 (1980), 1684; Surf.Sci. 125 (1983), 317.

[22] J.Q. Broughton and L.V. Woodcock, J.Phys. C 11 (1978), 2743.

[23] F. Ercolessi, thesis, University of Trieste (1983).

[24] R.A. Johnson, Phys.Rev. B 6 (1972), 2094.

[25] M.I. Baskes and C.F. Melius, Phys.Rev. B 20 (1979), 3197.

[26] M.W. Finnis, invited lecture at the NATO Advanced Research Workshop on the Chemistry and Physics of Fracture, Bad Reichenhall (1986).

[27] P. Wynblatt, Surf.Sci. 136 (1984), L51.

[28] A.H. MacDonald and R. Taylor, Can.J.Phys. 62 (1984), 796.

[29] M. Garofalo, thesis, International School for Advanced Studies, Trieste (1984).

[30] F. Ercolessi, E. Tosatti and M. Parrinello, Phys.Rev.Lett. 57 (1986), 719.

[31] M.S. Daw and M.I. Baskes, Phys.Rev.Lett. 50 (1983), 1285.

[32] M.S. Daw and M.I. Baskes, Phys.Rev. B 29 (1984), 6443.

[33] M.S. Daw and R.D. Hatcher, Sol.St.Comm. 56 (1985), 697.

[34] S.M. Foiles, Phys.Rev. B 32 (1985), 3409.

[35] M.S. Daw, Surf.Sci.Lett. 166 (1986), L161.

[36] S.M. Foiles, Phys.Rev. B 32 (1985), 7685.

[37] S.M. Foiles and M.S. Daw, J.Vac.Sci.Technol. A3 (1985), 1565.

[38] S.M. Foiles, M.I. Baskes and M.S. Daw, Phys.Rev. B 33 (1986), 7983.

[39] M.J. Stott and E. Zaremba, Phys.Rev. B 22 (1980), 1564.

[40] J.K. Nørskov, Phys.Rev. B 26 (1982), 2875.

[41] E. Clementi and C. Roetti, At.Data Nucl.Data Tables 14 (1974), 177.

[42] A.D. McLean and R.S. McLean, At.Data Nucl.Data Tables 26 (1981), 197.

[43] M.W. Finnis and J.E. Sinclair, Philos.Mag. A 50 (1984), 45; Erratum: Philos.Mag. A 53 (1986), 161.

[44] C.C. Matthai and D.J. Bacon, Philos.Mag. A 52 (1985), 1.

[45] G.J. Ackland and M.W. Finnis, Philos.Mag. A 54 (1986), 301.

[46] V. Heine, in Solid State Physics Volume 35, ed. by H. Ehrenreich, F. Seitz and D. Turnbull (Academic, New York, 1980).

[47] G. Allan, in "Handbook of surfaces and interfaces", Volume 1, ed. by L. Dobrzynski (Garland, New York,

1978), p. 299, and references therein.

[48] D. Tománek and K.H. Bennemann, Surf.Sci. 163 (1985), 503.

[49] K. Fuchs, Proc.Roy.Soc. A153 (1936), 622; A157 (1936), 444.

[50] D. Castiel, L. Dobrzynski and D. Spanjaard, Surf.Sci. 59 (1976), 252.

[51] V. Bortolani and G. Santoro, in Proc. of the Second Int. Conf. on Phonon Physics, ed. by J. Kollar, N. Kroo, N. Menyhard and T. Siklos (World Scientific, Singapore, 1985), p. 566.

[52] A.R. Miedema, Z.Metallk. 69 (1978), 287.

[53] J.R. Neighbours and G.A. Alers, Phys.Rev. 111 (1958), 707.

[54] J.W. Lynn, H.G. Smith and R.M. Nicklow, Phys.Rev. B 8 (1973), 3493.

[55] Am.Inst.of Phys. Handbook, 3rd ed. (McGraw-Hill, New York, 1972).

[56] M. Parrinello and A. Rahman, Phys.Rev.Lett. 45 (1980), 1196; J.Appl.Phys. 52 (1981), 7182.

[57] M. Parrinello, A. Rahman and P. Vashishta, Phys.Rev.Lett. 50 (1983), 1073.

[58] W.B. Pearson, "A handbook of lattice spacings and structures of metals and alloys", Volume 2 (Pergamon Press, Oxford, 1967), p. 648; the data set used is that of H. Warlimont, Z.Metallk. 50 (1959), 708.

[59] P. Carnevali, F. Ercolessi and E. Tosatti, in preparation.

[60] See, e.g., J.Q. Broughton and G.H. Gilmer, J.Chem.Phys. 79 (1983), 5095.

[61] L. Pietronero and E. Tosatti, Sol.St.Comm. 32 (1979), 255.

[62] Y. Waseda, "The structure of non-crystalline materials" (McGraw-Hill, Toronto, 1980), p. 276.

[63] see, e.g., C.A. Croxton, "Liquid state physics" (Cambridge University Press, 1974), sec. 5.9.

[64] A.M. Stoneham, "Theory of defects in solids" (Clarendon Press, Oxford, 1975), chapter 8.

[65] A.C. Damask and G.J. Dienes, "Point defects in metals" (Gordon and Breach, New York, 1963), chapter 5.

[66] J. Friedel, in "Vacancies and Interstitials in Metals", ed. by A. Seeger, D. Schumacher, W. Schilling and J. Diehl (North-Holland, Amsterdam, 1970), p. 787.

[67] D.G. Fedak and N.A. Gjostein, Phys.Rev.Lett. 16 (1966), 171.

[68] A.M. Mattera, R.M. Goodman and G.A. Somorjai, Surf.Sci. 7 (1967), 26.

[69] D.G. Fedak and N.A. Gjostein, Surf.Sci. 8 (1967), 77.

[70] P.W. Palmberg and T.N. Rhodin, Phys.Rev. 161 (1967), 586.

[71] P.W. Palmberg and T.N. Rhodin, J.Chem.Phys. 49 (1968), 134.

[72] D.M. Zehner, B.R. Appleton, T.S. Noggle, J.W. Miller, J.H. Barrett, L.H. Jenkins and O.E. Schow III, J.Vac.Sci.Technol. 12 (1975), 454.

[73] J.F. Wendelken and D.M. Zehner, Surf.Sci. 71 (1978), 178.

[74] M.A. Van Hove, R.J. Koestner, P.C. Stair, J.P. Bibérian, L.L. Kesmodel, I. Bartoš and G.A. Somorjai, Surf.Sci. 103 (1981), 189; Surf.Sci. 103 (1981), 218.

[75] K.H. Rieder, T. Engel, R.H. Swendsen and M. Manninen, Surf.Sci. 127 (1983), 223.

[76] G.K. Binnig, H. Rohrer, Ch. Gerber and E. Stoll, Surf.Sci. 144 (1984), 321.

[77] V. Heine and L.D. Marks, Surf.Sci. 165 (1986), 65.

[78] for a similar physical situation, see also J.A. Snyman and J.H. van der Merwe, Surf.Sci. 42 (1974), 190.

[79] F. Ercolessi, M. Parrinello and E. Tosatti, Surf.Sci. (to be published).

[80] P. Bak, Rep.Prog.Phys. 45 (1982), 587.

[81] H. Rohrer, private communication.

[82] Y. Kuk, private communication.

[83] M. Garofalo, E. Tosatti and F. Ercolessi, to be published.

[84] A. Bartolini, thesis, International School for Advanced Studies, Trieste (1986).

[85] X.Q. Wang and E. Tosatti, in preparation.

[86] W. Andreoni, F. Ercolessi and E. Tosatti, in preparation.

[87] A. Rahman, in "Correlation functions and quasiparticle interactions in condensed matter", NATO Advanced Study Institute Series, Volume B35 (Plenum, New York, 1977), p. 417.

APPENDIX
GLUE FORCES IN MOLECULAR DYNAMICS

A standard molecular dynamics program based on two-body interactions can be easily extended to include the glue forces (given by equation (13)); the number of computations required is roughly doubled.

The procedure requires two passes over all the interacting pairs [*]. In the first pass, the two-body forces and the total coordinations are calculated for each particle. In the second pass, the glue forces are computed. This splitting is necessary because all the coordination n_i must be known to calculate the glue forces.

The first pass can be schematized as follows (using pseudocode):

```
/*  Reset to zero arrays forcex, forcey, forcez, coord  */
do i=1,N-1
    do j=i+1,N
        /*  Compute the distance rij= sqrt(xij^2 + yij^2 + zij^2)  */
        /*  between particles i and j                              */
        if (rij<rc) then
            /*  Compute f = -(1/rij)φ'(rij)  */
            forcex(i) = forcex(i) + f*xij
            forcey(i) = forcey(i) + f*yij
            forcez(i) = forcez(i) + f*zij
            forcex(j) = forcex(j) - f*xij
            forcey(j) = forcey(j) - f*yij
            forcez(j) = forcez(j) - f*zij
        endif
        if (rij<rm) then
            /*  Compute rhoij = ρ(rij)  */
            coord(i) = coord(i) + rhoij
            coord(j) = coord(j) + rhoij
        endif
    enddo
enddo
```

An intermediate single loop is required at this point to calculate the first derivative of the glue as a function of the total coordination for each particle:

---

[*] By "interacting pairs", we intend here pairs of particles whose distance is less than $\max(r_c, r_m)$, where r_c is the range of $\phi(r)$ and r_m is the range of $\rho(r)$.

```
do i=1,N
    uderiv(i) = U'(coord(i))
enddo
```

In the second pass, the glue forces are added to the two-body forces calculated in the first pass:

```
do i=1,N-1
    do j=i+1,N
        /*  Compute the distance rij= sqrt(xij^2 + yij^2 + zij^2)  */
        /*  between particles i and j                              */
        if (rij<rm) then
            /*  Compute g = -(1/rij)ρ'(rij)  */
            f = g * ( uderiv(i) + uderiv(j) )
            forcex(i) = forcex(i) + f*xij
            forcey(i) = forcey(i) + f*yij
            forcez(i) = forcez(i) + f*zij
            forcex(j) = forcex(j) - f*xij
            forcey(j) = forcey(j) - f*yij
            forcez(j) = forcez(j) - f*zij
        endif
    enddo
enddo
```

Of course, a real world program should have some sort of bookkeeping mechanism, such as a neighbours list [87], to keep track of the pairs which are close enough to interact. This avoids the expensive computation of all the N(N-1)/2 distances at each time step. Due to the short range of the functions employed, the benefits of using this technique are very large when N is of the order of 1000 or more.

Also, it is suggested to use numerical tables for $\phi(r)$, $\rho(r)$, U(n), instead of calculating them analytically. By constructing the tables of $\phi(r)$ and $\rho(r)$ through a uniform sampling in r^2 rather than in r, the square roots computations can be avoided.